Speed Control of a PMSM for Three-Wheeler Electric Bajaj Using Integral Sliding Mode Control with Exponential Reaching law

Hamza Abdo

A Thesis Submitted to

Department of Electrical Power and Control Engineering

School of Electrical Engineering and Computing

Presented in Partial Fulfillment of the Requirement for the Degree of Master of Science in Electrical Power and Control Engineering (Control Engineering)

Office of Graduate Studies

Adama Science and Technology University

Sept 2024

Adama, Ethiopia

Speed Control of a PMSM for Three-Wheeler Electric Bajaj Using Integral Sliding Mode Control with Exponential Reaching law

Hamza Abdo

Advisor: Prof. Gang Gyoo Jin

A Thesis Submitted to

Department of Electrical Power and Control Engineering

School of Electrical Engineering and Computing

Presented in Partial Fulfillment of the Requirement for the Degree of Master of Science in Electrical Power and Control Engineering (Control Engineering)

Office of Graduate Studies

Adama Science and Technology University

Sept 2024

Adama, Ethiopia

DECLARATION

I hereby declare that this Master Thesis entitled " Speed Control of a PMSM for Three-Wheeler Electric Bajaj Using Integral Sliding Mode Control with Exponential Reaching law" is my original work. That is, it has not been submitted for the award of any academic degree, diploma, or certificate in any other university. All sources of materials that are used for this thesis have been duly acknowledged through citation.

Hamza Abdo Ribato	______	__________
Name of student	Signature	Date

RECOMMENDATION

I, the advisor of this thesis, hereby certify that I have read the revised version of the thesis entitled " Speed Control of a PMSM for Three-Wheeler Electric Bajaj Using Integral Sliding Mode Control with Exponential Reaching law" prepared under my guidance by Hamza Abdo submitted in partial fulfillment of the requirements for the degree of Master of Science in Electrical Power and Control Engineering, postgraduate in control engineering.

Therefore, I recommend the submission of revised version of the thesis to the department following the applicable procedures.

Prof. Gang Gyoo Jin	________________	______
Advisor	Signature	Date

APPROVAL SHEET

I, the advisors of the thesis entitled " Speed Control of a PMSM for Three-Wheeler Electric Bajaj Using Integral Sliding Mode Control with Exponential Reaching law" and developed by Hamza Abdo, hereby certify that the recommendation and suggestions made by the board of examiners are appropriately incorporated into the final version of the thesis.

<u>Prof. Gang Gyoo Jin</u>	__________________	_____________
Advisor	Signature	Date

We, the undersigned, members of the Board of Examiners of the thesis by Hamza Abdo have read and evaluated her thesis entitled " Speed Control of a PMSM for Three-Wheeler Electric Bajaj Using Integral Sliding Mode Control with Exponential Reaching law" and examined the candidate during open defense. This is, therefore, to certify that the thesis has been accepted in partial fulfillment of the requirement of the Degree of Masters in control engineering

_____________._____________	____________________	____________
Chairperson	Signature	Date
_____________._____________	____________________	____________
Internal Examiner	Signature	Date
_____________._____________	____________________	____________
External Examiner	Signature	Date

Finally, approval and acceptance of the thesis is contingent upon submission of its final copy to the Office of Postgraduate Studies (OPGS) through the Department Graduate Council (DGC) and School Graduate Committee (SGC)

_____________._____________	____________________	__________
Department Head	Signature	Date
_____________._____________	____________________	__________
School Dean	Signature	Date
_____________._____________	____________________	__________
Office of Postgraduate Studies, Dean	Signature	Date

ACKNOWLEDGEMENT

I am deeply thankful to God for providing me with the courage and determination to finish my thesis. I am extremely appreciative of my advisor, Prof. Gang Gyoo Jin, for his continuous support, helpful guidance, and constant encouragement. His knowledge and feedback were very important to my research. I also want to show my family my appreciation, friends, and coworkers for having faith in me and supporting me. Their encouragement motivated me a lot. Lastly, I appreciate Dire Dawa University for allowing me to study for my master's degree at ASTU.

Table of Contents

LIST OF FIGURES

LIST OF TABLES

LIST OF ACRONYMS

AC	Alternating Current
BLDC	Brushless DC motor
BLDCM	Brushless Direct Current Motor
DC	Direct Current
EMF	Electro Motive Force
EV	Electric Vehicle
FOC	Field-Oriented Control
FOSMC	Fractional Order Sliding Mode Controller
GA	Genetic Algorithm
HEV	Hybrid Electric Vehicle
IFSMC	Integral Fixed-time Sliding Mode Controller
IM	Induction Motor
ISMC	Integral-Sliding Mode Controller
ISMC-ERL	Integral sliding mode control with exponential reaching law
LTI	Linear Time Invariant
MATLAB	Matrix Laboratory
NDOB	Novel non-linear Disturbance Observer
PI	Proportional Integral
PID	Proportional Integral Derivative
PMSM	Permanent Magnet Synchronous Motors
PWM	Pulse Width Modulation
SMC	Sliding Mode Control
SRM	Switched Reluctance Machines
SVPWM	Space Vector Pulse Width Modulation
SVM	Space Vector Modulation
V/F	Volt per Frequency
VSI	Voltage Source Inverter

LIST OF SYMBOLS

B	Viscous friction coefficient.
C_r	Rolling friction coefficient
η	Efficiency
E_{abc}	Three-phase induced EMF
F_r	Rolling friction force
F_g	Gravitational force
F_a	Aerodynamic force
g	Gravitational acceleration
i_{abc}	Three-phase current
i_{d}, i_q	d,q-axis stator current
L_{d}, L_q	d,q-axis stator inductance
J	Rotor moment of inertia
M	Vehicle gross mass
P	Number of poles
R	Stator resistance.
R_s	Stator resistance
T_e	Electromagnetic torque
T_L	Torque Load
$s(t)$	Sliding surface.
V_{dc}	Dc-link voltage
V_{abc}	Three phase voltage
V_d, V_q	d, q component voltage
λ_d, λ_q	d, q component stator-flux linkage.
ρ	Density
ω_r	Rotor speed of the motor
θ_r	Position of the rotor
α	Alpha
β	Beta

ABSTRACT

Electric vehicles (EVs) provide a potential solution for decreasing fossil fuel consumption and air pollution, thereby promoting sustainable transportation. However, optimizing energy efficiency and utilization remains a critical challenge. Permanent Magnet Synchronous Motors (PMSMs) are recognized for their superior efficiency compared to other electric drive systems, despite their complex control requirements. This thesis proposes an Integral-Sliding Mode Control (ISMC) with Exponential Reaching Law (ISMC-ERL) for PMSM drives in EVs to achieve robust speed regulation and eliminate chattering. The controller's performance was evaluated through MATLAB/Simulink simulations, considering speed tracking, load variations, and operation at different speeds. Comparative analysis with conventional SMC and PID controllers demonstrated the superior performance of ISMC-ERL, characterized by a rapid rise time of 0.0019 seconds, a settling time of 0.0032 sec, and a minimal overshoot of 1.67%

Key Words: EV, PMSM, ISMC-ERL, PID controller

CHAPTER ONE
INTRODUCTION

1.1 Background

The popularity of electric vehicles has grown significantly in recent years, making them a desirable choice for sustainable and energy-efficient transportation. (Cao et al., 2012). The performance of the drive motor is crucial for a vehicle's maneuverability, safety, and overall driving experience. EVs frequently employ permanent magnet synchronous motors (PMSMs), yet their operation can be complex, influenced by varying motor parameters and environmental conditions. Improving the drive motor's dynamic response and robustness is therefore a critical research area. As the propulsion system's core component, EV traction motors demand High torque, power density, speed range, efficiency, reliability, quiet operation, and affordability.

The permanent magnet synchronous motor (PMSM) has made substantial prominence in the industry standard for high-performance applications including electric automobiles and machine tools. Distinguished by its simple construction, compact dimensions, and lightweight profile, the PMSM is exceptionally well-suited to the space constraints inherent in electric vehicle design. Moreover, the motor's low inertia contributes to its overall efficiency and responsiveness (Lee, 2009). The PMSM's exceptional power density, a measure of the motor's power output relative to its size, has solidified its position as a leading candidate for electric vehicle propulsion systems. This characteristic, coupled with the increasing global emphasis on environmental sustainability and energy conservation, has spurred substantial investment in PMSM technology for both electric vehicles and renewable energy applications. To harness the full potential of PMSM-driven systems, advanced control strategies are essential (Jiacai et al., 2012). Field-oriented control (FOC) has become a standard approach for regulating PMSM operation. This method involves employing a Proportional-Integral (PI) controller to manage motor speed. However, to optimize system performance and mitigate issues such as overshoot and oscillations, the inclusion of a derivative term in the control loop is often necessary. This derivative component enhances the controller's ability to damp out transient responses, resulting in smoother and more precise motor control.

PID controllers stand as the most ubiquitous and widely applied control strategy in industrial settings. Their versatility has led to their implementation across a broad spectrum of dynamic systems, encompassing industrial processes, aviation, and marine systems. The enduring popularity of PID, or three-term controllers, is primarily attributed to their simplicity and effectiveness. The proportional (P) and derivative (D) terms contribute to system stability and transient response, while the integral (I) term ensures accurate tracking of setpoint values (Pathak et al., 2020). When properly tuned, PID controllers deliver robust and reliable efficiency in a variety of applications. Operating as a feedback control mechanism, the PID controller continuously monitors the system's output and calculates an error signal relative to the desired setpoint. Based on this error, to be able to change its input and move the output in the direction of the desired value, the controller produces a control signal.

Electric motor speed and position can be regulated with the help of a control technique called sliding mode control (SMC). It has a reputation for being adaptable and having fast reaction times. Chattering, on the other hand, is a significant disadvantage of SMC and arises when the control signal abruptly changes on and off. (Pathak et al., 2020). This can cause problems like reduced accuracy and damage to the motor.

1.2 Statement of the Problem

While an increase in vehicle manufacturers can contribute to economic growth, it also raises concerns about rising greenhouse gas emissions. To create a healthy environment, reducing these emissions is essential. Traditional vehicles primarily rely on fossil fuels, a significant cause of air pollution and harmful gases. Another limited resource that is experiencing price hikes and depletion is fossil fuels. To address these challenges, electric vehicles (EVs) are emerging as a promising alternative. However, for EVs to be truly sustainable, overcoming energy efficiency limitations and optimizing energy utilization is crucial, while also lowering the environmental footprint of EVs. The motor has a crucial function in an electric vehicle, requiring an efficient and precise control system. Because of their higher efficiency compared to other electric drives, Permanent Magnet Synchronous Motors (PMSMs) are frequently selected. For optimal performance, especially during fast braking and torque control, an accurate model and simulation of the PMSM drive, particularly its speed control, is essential. This ensures efficient energy use and smooth operation of the electric vehicle.

1.3 Objective

1.3.1 General Objective

The primary goal of this thesis is to develop and analyzed the performance an integral-SMC (ISMC) technique that uses ERL to give PMSMs the best possible speed control.

1.3.2 Specific Objective

The specific goals of this thesis are: -

- To examine the dynamics of electric vehicles and their mathematical model.
- To study the PMSM's properties and modeling for an EV drive system.
- To design and analyze an ISMC-ERL speed control law based on the PMSM drive system's nonlinear model.
- To tune controller parameters with a genetic algorithm.
- Simulate and evaluated the overall speed control performance under various scenarios, comparing it with two other control methods.

1.4 Scope

The development of mathematical models for permanent magnet synchronous motors (PMSMs) is the main topic of this thesis. Integral Sliding Mode Control (ISMC) is used in the development and assessment of a speed controller for PMSM-driven electric vehicles (EVs). Through simulation, the controller's performance of PMSM speed was compared to conventional SMC and PID controllers, using MATLAB/Simulink for simulation and analysis the result.

1.5 Significance

Energy wastage and air pollution have long been pressing global and national challenges. In response, the world is transitioning from non-renewable to renewable energy sources, particularly in the transportation sector. By swapping out gasoline-powered cars for electric vehicles, we can greatly minimize air pollution and energy consumption associated with electric vehicles.

1.6 Limitations

Given the constraints of brief duration, system complexity, and material costs, the development of a physical prototype was infeasible. Consequently, this research focused on simulation employing MATLAB/Simulink software, and the system's intended performance was evaluated in a simulated environment without practical implementation.

1.7 Motivations

A major transformation is underway in the automotive industry, with a growing focus on electric vehicles (EVs) driven by concerns about energy consumption and environmental impact. Electric vehicles rely on electric motors for propulsion, demanding high-performance components capable of delivering wide speed ranges, strong dynamic performance, and high efficiency. Among various motor technologies, the superior efficiency of Permanent Magnet Synchronous Motors (PMSMs) makes them stand out., compact size, robust torque-speed characteristics, extended lifespan, and versatility. Consequently, PMSM drives have found widespread applications in electric vehicles, robotics, aerospace, and industrial systems.

1.8 Thesis Organization

This thesis consists of six chapters.

Chapter 1: In the first chapter discussed an overview of electric vehicles and electric motor drives, outlining the thesis' objectives and scope.

Chapter 2: Provides a thorough review of relevant research on permanent magnet synchronous motor drives and their control techniques.

Chapter 3: Develops dynamic models for both the PMSM drive and the EV, incorporating Field Oriented Control (FOC) based on coordinate transformation.

Chapter 4: Designs and analyzes speed and current controllers for the PMSM drive system.

Chapter 5: The simulation results of the developed system are examined in detail in this chapter, along with their potential implications.

Chapter 6: The final chapter concludes the thesis by summarizing key findings, drawing meaningful conclusions, and outlining potential recommendations.

CHAPTER TWO
LITERATURE REVIEW

2.1 Introduction

A comparative analysis of PMSM performance against other electric motor types is presented in this chapter, highlighting the advantages and disadvantages of each. It explains the common control strategies employed for PMSM operation and provides a comprehensive review of existing research on PMSM speed control techniques.

2.2 Electric Vehicles

Electric drives systems enable the regulated transformation between electrical and mechanical forms by adjusting magnetic fields. Fundamental concepts from electric drive systems form the basis of AC motor control. The direction, torque, and speed of moving objects are all controlled by these mechanisms. Electric drives regulate electric motors and are mostly used for speed or motion control. Although variable speed drives provide operation over a wide speed range, constant speed drives are sufficient for static applications. Variable speed drives offer various other advantages as listed in the following: they offer accurate and continuous control over current, speed, position, or torque for a variety of loads. (Abu-Rub et al., 2021).

2.3 Types of Electric Motors

To meet the demands of electric vehicles, motors must exhibit a combination of high-power density, efficiency, overload capability, and durability. Power density and efficiency are paramount for propulsion systems. Optimal motor performance, particularly in frequently used driving conditions, is crucial. However, balancing efficiency gains with cost reduction and size minimization presents a significant challenge (Bello et al., 2020). Electric vehicle (EV) propulsion systems utilize a variety of motor technologies, including induction, switching reluctance, DC, BLDC, and permanent magnet synchronous (PMSM) motors (Bhatt et al., 2019). PMSM motors are often preferred due to their high efficiency, resulting from the absence of rotor windings, copper losses, and commutators, which collectively contribute to reduced maintenance and increased power density (Nanda & Kar, 2006).

2.3.1 Performance Comparison of Electric Motors

A variety of electric motors can propel electric vehicles, but their suitability varies based on specific characteristics such as advantages, disadvantages, and performance limitations influence the choice of motor for electric propulsion applications. Table 2.1 provides a comparative analysis of different electric motor types (Hashemnia & Asaei, 2008; Zeraoulia et al., 2006).

Table 2.1**:** Analysis of Motors Used in EVs: Advantages and Disadvantage

Motors	Advantage	Disadvantage
IM	Outstanding dynamics and appropriate control Possibility of high-speed operating Lower cost and easier to assemble	Less effectiveness when the load is lighter Intricate control Power factor is always trailing
SRM	Excellent properties of torque-speed Large constant power zone and high fault tolerance Possess an uncomplicated, inflexible structure	Unique converter topology is required. Possess large torque ripple and noise Sophisticated control system.
DC	Maximum torque when moving slowly Excellent controllability Minimal torque ripple Curve of linear torque-current	Poor dependability Needs upkeep Limited ability to overload
BLDCM	Exceptional power output and a high torque-to-inertia ratio. Outstanding thermal management and overload resistance.	Expensive Torque ripple Low-quality file deterioration
PMSM	High effectiveness and Smooth torque Strong overload resistance and efficient heat dissipation Excellent filed weakening ability	Expensive

2.3.2 Permanent Magnet Synchronous Motors (PMSM)

Both PMSMs and BLDC motors utilize permanent magnets on their rotors to generate torque. However, they distinguish themselves by their unique back EMF waveforms. PMSMs produce a smooth, sinusoidal EMF, while BLDC motors generate a stepped, trapezoidal EMF.

Due to their inherent advantages, PMSMs have become the favored option for medium-power AC motor applications. Their exceptional performance has driven widespread adoption in drive technologies. Consequently, PMSMs are increasingly integrated into various industrial systems, from basic pumps and fans to demanding electric vehicle (EV) propulsion systems. Their Exceptional power output and a high torque-to-inertia ratio, and efficacy, coupled with a robust design, low production costs, and excellent dynamic response make them ideally suited for the rigorous demands of EV operation. PMSM have the following characteristics (Ramu Krishnan, 2017):

- Sinusoidal airgap field intensity
- Sinusoidal wave current
- Sinusoidal stator conductor arrangement

2.4 Control Techniques of PMSM

The two main control strategies used by PMSM control systems are vector and scalar. Scalar control is simple, although, its performance limitations have led to the widespread adoption of vector control. Vector control offers superior performance by enabling independent control of the PMSM's flux and torque components (Parmar et al., 2016; Zeraoulia et al., 2006).

2.4.1 Scalar Control Technique for PMSM

Scalar control regulates motor speed by adjusting only the magnitude of the voltage and frequency. While simple to implement, this method lacks feedback, resulting in poor performance. Often referred to as volt/frequency control, it maintains a constant voltage-to-frequency ratio across the motor's operating range (Blaha & Václavek, 2012).

The desired synchronous speed determines the output frequency, while the voltage or current magnitude is adjusted to maintain a constant V/f ratio (Blaha & Václavek, 2012). This open-loop control method operates without motor parameter feedback, simplifying the system and eliminating the need for sensors.

The synchronous speed of the motor is calculated as:

$$W_s = \frac{2\pi f_s}{p} \tag{2.1}$$

where W_s is the synchronous speed (rad/s), f_s is the line voltage frequency (Hz), and p is the number of poles. Electric vehicle traction motors require advanced control strategies for optimal performance. Given its poor dynamic response, scalar control is unsuitable for the demanding requirements of permanent magnet motors in electric vehicles.

2.4.2 Vector Control for PMSM Drives

Vector control is a PMSM control technique comprising a motor, inverter, speed controller, and coordinate transformations (Suman & Mathew, 2018). It excels in dynamic reaction, precision, and broad speed range, but is susceptible to motor parameter variations (Liu et al., 2015). Unlike scalar control, vector control employs motor parameters like position or speed as feedback for enhanced performance.

The Park and Clarke transformations are utilized by vector control, sometimes referred to as field-oriented control, to split three-phase stator currents into d-q components. This method combines two closed-loop control frameworks. While the inner for regulates d-q currents, outer controls the motor's speed or position. Figure 2.1 displays the field-oriented control block diagram.

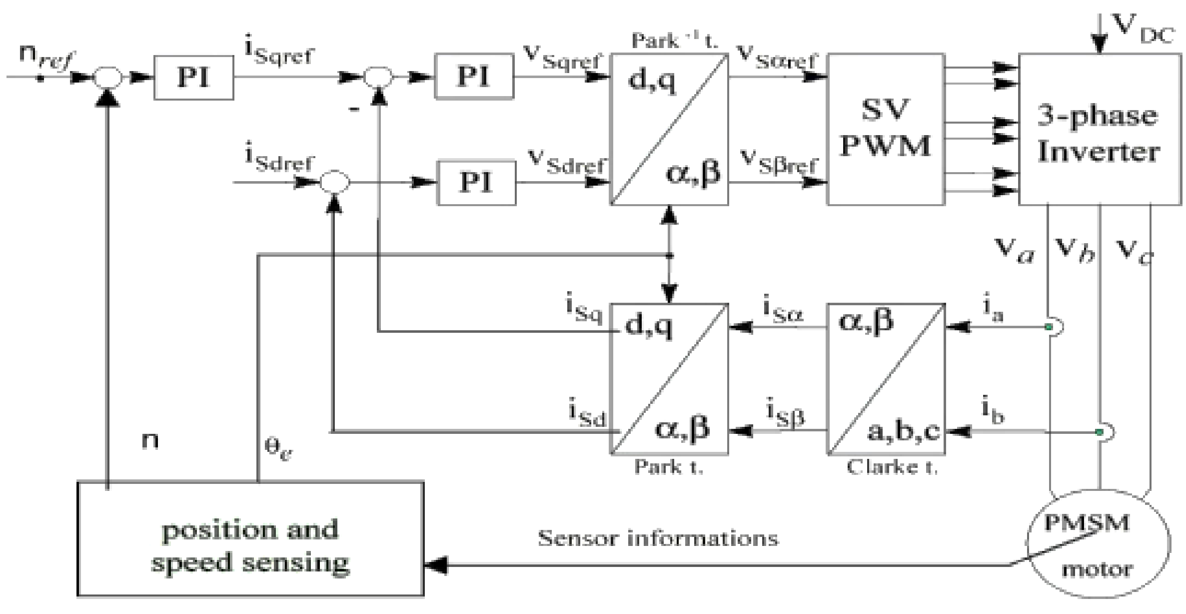

Figure 2.1: Vector control schematic illustration for PMSM (Liu et al., 2015).

2.5 Sliding Mode Controller Enhancement in PMSM Speed Control

Chattering phenomena in sliding mode control are said to be the main obstacle for SMC to become one of the significant discoveries in modern control theory (Young et al., 1999). Researchers have proposed various methods to overcome this issue, whereby in doing so, the controller's performance in terms of disturbance rejection properties and/or tracking was also affected, either in an advantageous or deteriorative way. Conversely, the proposed controller enhancement methods also determine the resulting chattering phenomena.

2.5.1 Sliding Surface Design Modification

New sliding surface designs have been proposed in many previous works in order to enhance the performance of SMC instead of using the conventional linear sliding surface. Linear sliding surface as in Equation (2.2) guarantees sliding mode asymptotic stability with convergence rate depending on the value of c (Zhang et al., 2013). The remarkable advantage of this design is its simplicity. However, the performance of conventional linear sliding surfaces is proven to be less satisfactory in terms of convergence rate and settling time. The dynamic response of a closed loop system can be improved by using nonlinear sliding surfaces. For PMSM speed control, several works have been executed using linear SMC, but the drawbacks of linear SMC were overcoming by means of hybridization to develop a composite SMC controller or modification of the reaching law (Zhang et al., 2013).

$$s = cx_1 + x_2, c > 0 \tag{2.2}$$

2.5.2 Integer Order Integral SMC

In conventional sliding mode control, the robustness of the system against parameters variation and external disturbances is achieved in the sliding phase. Prior to that, i.e., during the reaching phase, the robustness is not guaranteed. Integral sliding mode control (ISMC) (Equation (2.3)) was introduced by Utkin and Jingxin (Utkin & Shi, 1996) to overcome this problem by eliminating the reaching phase, therefore, sliding phase is enforced throughout the entire system response. Furthermore, the order of motion equation in integral SMC is not reduced by the control input dimension, but equal to the order of the original system. The control law consists of a continuous nominal control and discontinuous control, which is responsible for the performance of the nominal system without perturbations and for rejecting perturbations respectively. Hence, with this type of SMC, system robustness can be guaranteed from the initial time. In addition, smaller maximum control magnitude is required for ISMC than conventional SMC since the value is usually bigger during the reaching phase (Castanos & Fridman, 2006).

$$s = e(t) - \int_0^t (a + bK)e(\tau)d\tau \tag{2.3}$$

2.5.3 Fractional Order SMC

Another nonlinear sliding surface design method is the fractional order sliding surface, which utilizes fractional calculus in constructing its sliding surface. Fractional calculus emerged theoretically over 300 years ago, but in recent decades it has been applied practically in a wide range of science and engineering disciplines (Efe, 2011). It is a generalization of the traditional integer order integration and differentiation to the non-integer order. Fractional order terms have the property of attenuating old data and storing new data, hence they are more stable or at least as stable as their integer order counterparts (Huang et al., 2014). Fractional calculus has been extensively integrated with classical PID control theory to come out with fractional PID controllers indicated as PIλDμ. Other fractional order controller includes fractional adaptive controllers, fractional order compensators, fractional order sliding mode observer and fractional order sliding mode control (FOSMC) (Mujumdar et al., 2015).

$$s = k_p e(t) + {}_0D_t^r e(t) \tag{2.4}$$

$k_p > 0; {}_0D_t^r(\cdot)$ is fractional order integral with $0 < r < 1$

2.5.4 Higher Order SMC

Higher order sliding mode control (HOSMC) was first introduced by Levant (LEVANT, 1993). In first order SMC, the selected sliding surface has a relative degree one with respect to the control input. The control input acts on the first derivative of the sliding surface. In higher order SMC, the control input acts on higher derivatives of the sliding surface. A sliding mode is defined as n-th order sliding mode when Equation (2.5) is satisfied (Eker, 2010). The n-th derivative is predominantly supposed to be discontinuous or nonexistent. The sliding order characterizes the system dynamics in the vicinity of the sliding mode in terms of degree of smoothness (LEVANT, 1993). In literatures, various sliding surface types were used in designing their HOSMC. Reset numbering

$$s(t) = \dot{s}(t) = \cdots = s^{(n-1)}(t) = 0 \tag{2.5}$$

2.6 Related Work of Studies

PMSM motor drives have captivated researchers for the past three decades (Maji et al., 2015). To enhance drive motor control performance, extensive research has focused on PMSM speed control. Technological developments in semiconductors, magnetic materials, and microprocessors have made it easier for AC motors to be widely used in high-speed drive systems. Owing to their inherent advantages, PMSMs have emerged as the dominant choice for medium-power AC motor applications.

The paper (Benzaouia et al., 2022) presents a robust control strategy for Permanent Magnet Synchronous Motors (PMSMs) in electric vehicles. By combining the advantages of integral sliding mode control and an exponential reaching law, the proposed method offers improved disturbance rejection, faster transient response, and reduced chattering compared to traditional control techniques. The paper likely provides theoretical analysis, simulation results, and potentially experimental validation to demonstrate the effectiveness of the proposed control approach in enhancing the performance and reliability of PMSM-driven electric vehicles. However, there is a chattering issue of chattering, it is not completely eliminate chattering, especially in the presence of significant disturbances or parameter uncertainties.

Authors in (Xia et al., 2011), This study introduces innovative Integral Sliding Mode Control (ISMC) strategies to enhance disturbance rejection in PMSM speed control systems. While traditional ISMC methods often struggle to balance chattering and anti-disturbance performance, our proposed approaches effectively address these challenges. First, they present a linear varying gain ISMC that allows for reduced switching gain without compromising steady-state performance or disturbance rejection. Second, they develop an ISMC based ESO. ESO estimates both system states and disturbances, enabling feedforward compensation and reducing chattering. Third, they propose an adaptive control method leveraging the strength of linear varying gain and ESO. Results from experiments and simulations show how effective these improved methods in mitigating chattering while preserving dynamic performance and disturbance rejection. Although chattering is significantly reduced, it's not entirely eliminated in the existing work. So, to address this, we suggest exploring higher-order sliding mode techniques that involve transferring discrete elements to output variable higher derivatives.

The authors in (Suman & Mathew, 2018) compared the performance of PI, PID, SMC, and combined SMC-PID controllers for PMSM speed control. The authors employed vector control and MATLAB/Simulink for simulation. Results indicated that PID controllers excel at higher speeds, while PI controllers struggle, exhibiting instability. SMC outperformed traditional PI and PID controllers Regarding overshoot and settling time and robustness to parameter variations. Although the SMC-PID combination demonstrated superior speed control, the chattering effect induced by the SMC component significantly impacted the quadrature axis current, rendering it impractical for real-world applications.

The author in (Mohd Zaihidee et al., 2019), evaluated the performance of a fractional-order sliding mode controller with PID (FOSMC-PID) for PMSM drive speed control at 500 rpm and 2 Nm load torque. Comparisons were made with conventional integral sliding mode control (ISMC). The results indicated that FOSMC-PID exhibited significantly lower overshoot (9.22%) and shorter settling time (30 times) compared to ISMC. Additionally, the study compared FOSMC controllers with different sliding surface designs (PI, PD, PID), as presented in Table 2.2. The findings revealed that FOSMC with PID outperformed the other configurations. However, a notable limitation of this work is the insufficient reduction in chattering.

Table 2.2**:** FOSMC with different Controller Performance Comparison (Mohd Zaihidee et al., 2019)

Performance indices	SMC	FOSMC-PI	FOSMC-PD	FOSMC-PID
Overshoot [%]	9.22	5.52	0	0.8593
Settling time (sec)	0.0288	0.0094	0.096	0.0096
Speed drop (V)	1.28	4.3	1.5	1.16
Steady state error (rpm)	0.02	0.04	0.06	0.02
Torque ripple	12	11	10	10
Speed ripple	0.16	0.12	0.014	0.014

The authors in (Ding et al., 2014) proposed using sliding mode techniques to provide a combined speed detection and control solution for PMSM. A variable-structure model reference adaptive system (MRAS) speed observer was used in place of mechanical sensors. A sigmoid function replaced the signum function to reduce chattering. In addition, a sliding mode speed controller was used in place of a traditional PI controller to improve performance. Simulation results demonstrated rapid and accurate speed tracking, improved dynamic response, and elimination of speed overshoot. However, the proposed method did not fully address the chattering issue, and the sensor-less approach's reliance on accurate rotor position estimation remains a challenge.

The authors in (Kapil Parkh, 2014), propose a better space vector modulation method for PMSM FOC with the aim of enhancing PMSM performance in the FOC framework by optimizing pulse production. While PI controllers are commonly used for FOC, the authors acknowledge their limitations in handling system nonlinearities. However, the specific improvements proposed to address these limitations are not clearly outlined in the paper.

In (Yong, 2017), to optimize the performance of PMSM fans in new energy vehicles, a vector control strategy is presented. The authors used standard control procedures and a mathematical model of the PMSM to create a control system. A microcontroller, MC9S12ZVMC128, was employed to implement the vector control algorithm. The control software architecture included state machine-based management for start-up, open-loop, closed-loop, and fault conditions. While the experimental results demonstrated efficient and stable PMSM operation, its limited adoption was due to the motor's expensive cost.

Authors in (Zaihidee et al., 2019) because of their increased efficiency, PMSMs are gradually taking the place of induction motors. PMSMs, with their time-varying characteristics, complicated dynamics, and nonlinearity, require speed controllers that can precisely track, respond quickly, minimize overshoot, and effectively reject disturbances. A tried-and-true reliable control technique for systems vulnerable to disturbances and changes in parameters is SMC. With the aim of improve robustness and suppress chattering, this work emphasizes sliding surface design and composite control algorithms in its thorough review of the application of SMC to PMSM speed control. Through simulation findings, the efficacy of fractional-order sliding surfaces is investigated. However, guaranteeing convergence to the sliding surface, minimizing the reaching phase, and lowering chattering during sliding mode are the primary shortcomings of our work.

The authors in (Wang et al., 2020) introduces a new control technique for controlling the rotational speed of PMSM. Through improved convergence rate and disturbance rejection capability, the authors hope to enhance PMSM speed regulation systems' dynamic performance. Their proposal for PMSM speed regulation involves the use of an IFSMC algorithm. Within the study, the IFSMC law is developed using Lyapunov stability analysis and a suitable integral fixed-time sliding mode surface is designed. The suggested IFSMC technique can guarantee that the error in the speed tracking convergences to a limited area within a predetermined timeframe, therefore enhancing the system's dynamic response. In comparison to other current control techniques, the The outcomes of the simulation indicate how effective the suggested IFSMC technique is nevertheless, the work is deficient in a few crucial areas that would have improved the suggested approach's usefulness and contribution. The study lacks a thorough examination of the suggested IFSMC method's resilience to external disruptions and uncertainty in the parameters. which are common issues in PMSM systems. Secondly, the comparison is limited to conventional sliding mode control.

The authors in (Li et al., 2020) this study enhances PMSM speed control under uncertain parameters and time-varying load torque situations by using a novel nonlinear disturbance observer (NDOB)-based integral sliding mode control (ISMC) strategy. Calculating the aggregate disturbances present in the speed and current loops is accomplished by three different NDO designs. The predicted disturbances are then utilized to create an integral SMC. While the speed tracking error converges to zero, theoretical analysis ensures the asymptotic stability of the closed-loop system. Empirical findings confirm the efficacy of the suggested control strategy. While the authors do not offer a thorough comparison with other SMC approaches for PMSM control that are currently in use that are based on disturbance observers. This work's uniqueness and contributions would be reinforced by a more thorough comparison with the latest research.

While previous research has investigated PMSM speed control using various control techniques, several critical aspects, such as system response to varying reference speeds and dynamic load conditions, have been under-explored. Additionally, the current regulation component within the overall control system has often been overlooked. This study addresses these gaps by proposing an ISMC-ERL speed controller and a PI current controller. A thorough examination of the system's behavior under various operating situations is performed to evaluate how well the suggested control technique works.

CHAPTER THREE
MATERIAL AND METHODOLOGY

3.1 Overview of the Chapter

This chapter covers the mathematical modeling of a PMSM, as well as transformation (Clark and Park) and motor driving units like SVPWM-based inverters. The identified motor specification and the dynamics of the vehicle are analyzed. Additionally, an explanation of the system's general block diagram is provided.

3.2 Materials

This research employed several software applications. MATLAB, a versatile computing environment equipped with specialized toolboxes and Simulink, was utilized for simulations and analysis. Microsoft Office suite was instrumental in creating and formatting the thesis document. Math Type facilitated the incorporation of complex mathematical equations into both the thesis and accompanying presentations. Mendeley is used to manage and format citations within the thesis document and generate a standardized reference list.

3.3 Methods

This study comprises several key stages, outlined in Figure 3.1. Initially, a comprehensive literature review was conducted on electric vehicles, PMSM drives, and associated control techniques to provide a solid framework for the study. Subsequently, a mathematical model was developed for both the three-wheeled electric Bajaj vehicle and the permanent magnet synchronous motor. Utilizing MATLAB/Simulink, speed and current controllers were created and simulated based on the established PMSM model. The last phase involved a thorough performance evaluation of the speed control system under various operating conditions, including comparative analysis with other relevant controllers.

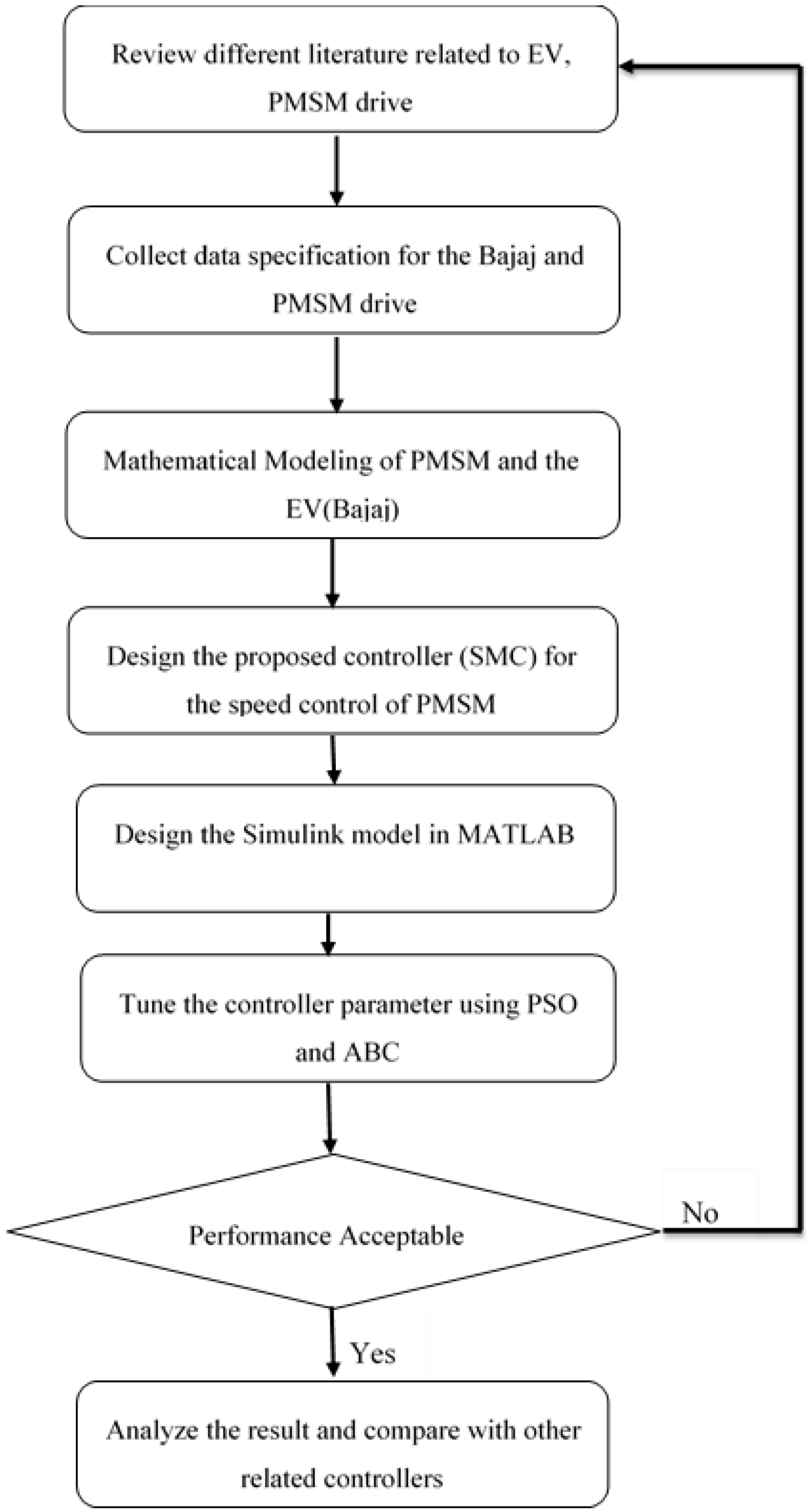

Figure 3.1 A Flow Chart Illustrating the Study Approach

3.4 System Block Diagram and Its Description

Figure 3.2 illustrates the proposed system's architecture, featuring a cascade control structure composed between an internal current controller and an external speed controller.

The target speed (ω_{ref}) is constantly comparing to the actual motor speed (ω) to function as a whole. The speed controller receives the speed error that is produced. Minimizing this speed inaccuracy is the aim of the speed controller, which is implementing an ISMC-ERL technique in this instance.

The speed controller's output serves as the target value for the current controller. The system incorporates a PI current controller to reduce the possibility of excessive beginning currents, which could cause overheating and other problems. This controller generates a voltage reference in the d-q coordinate frame. Subsequently, an inverse Park transformation converts the d-q reference voltages into the αβ frame. Finally, the obtained αβ reference voltages are applied to a SVPWM inverter to control the power switches' on and off.

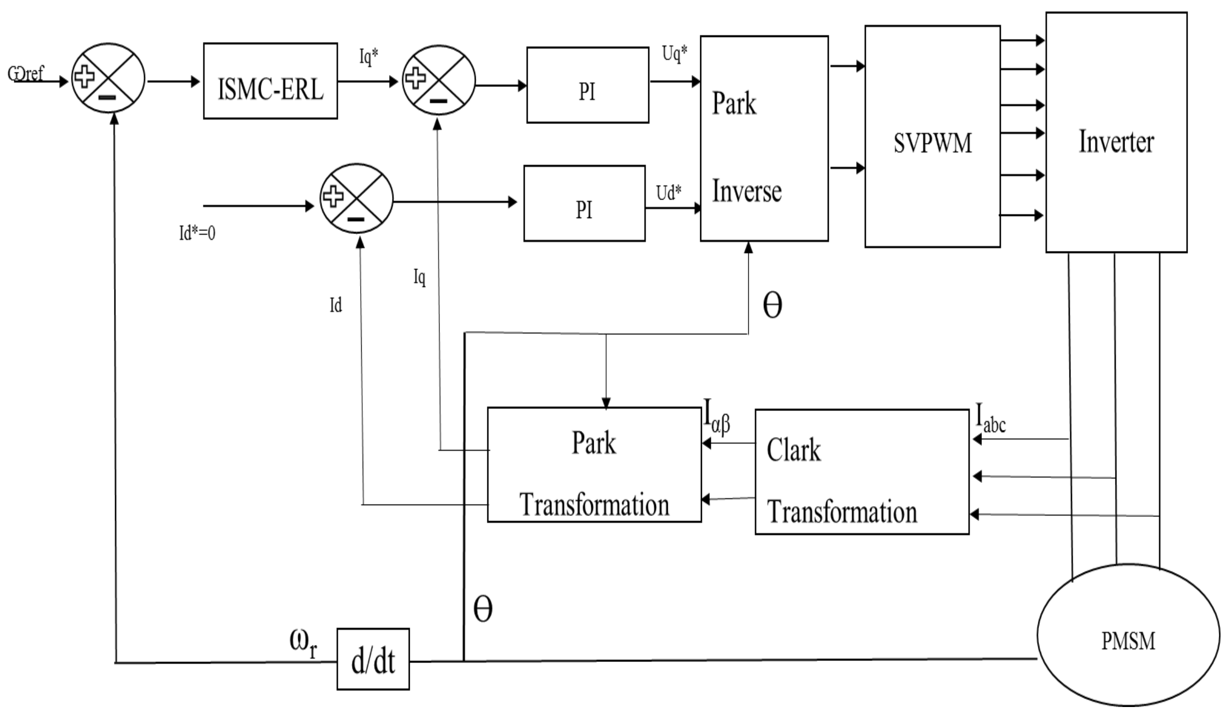

Figure 3.2 The Block Schematic That Shows the Suggested System.

The battery stores energy as DC, but the traction motor needs an AC power source. An inverter fills this voltage gap by converting the DC output of the battery into the required AC voltage. A two-phase representation of the three-phase motor system is introduced to streamline calculations and control design. The Clark transformation converts the three-phase system into the α-β stationary reference frame, while the Park transformation further transforms it into the d-q rotating reference frame.

3.5 EV Dynamics Model

3.5.1 Selection of Power Rating of PMSM for EVs

The transportation sector has placed a high priority on creating vehicles that are safe, economical, and environmentally friendly in recent years. Promising substitutes for traditional cars include fuel cell vehicles, EVs, and HEVs. A vehicle's motion is directly influenced by the forces acting upon it. To overcome resistances such as tire rolling friction, electric vehicles require suitably sized motors. Accurate motor selection necessitates a comprehensive analysis of vehicle dynamics, including factors like road conditions, aerodynamic drag, and rolling friction to determine the maximum torque requirements. The vehicle’s propulsion system provides the force necessary to move the vehicles forward. The vehicle can overcome the opposing forces caused by gravity, air resistance, and tire resistance thanks to this constraint of the propulsion unit (Chauhan, 2015). The proposed three-wheel Bajaj are shown in Figure 3.3.

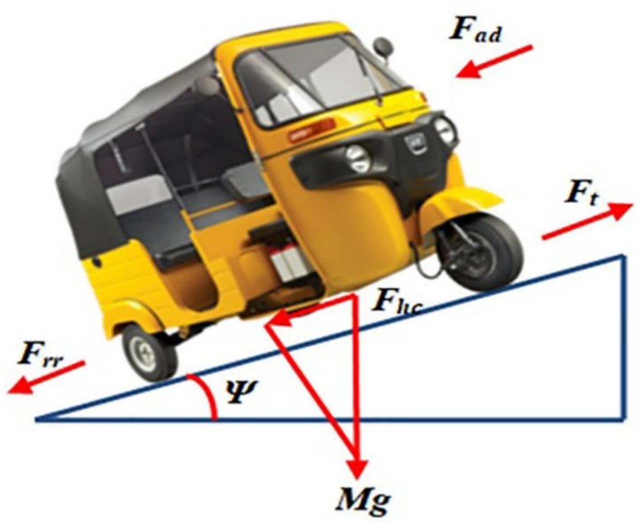

Figure 3.3 Force acting on a vehicle during uphill drive (Vidhya & Mahadevan, 2019)

The main forces that must be overcome to propel an electric vehicle are:

1. Rolling friction force
2. Aerodynamics drag force
3. Slope resistance force

Rolling friction force

The force that prevents a car from moving due to the interaction of the tires with a road is referred to as rolling friction. This resistance is influenced by factors such as tire material and road condition, which affect the rolling friction coefficient (Chauhan, 2015; R. & Rajagopal, 2016). The rolling friction can be calculated as:

$$F_{rr} = C_{rr} W \cos\theta \tag{3.1}$$

where F_{rr} is the rolling friction, C_{rr} is coefficient of rolling friction, W is the gross weight of the vehicle (Mg), *M is* the vehicles' mass, g is the gravitational acceleration, and Angle of inclination is θ.

By inputting the parameter values into Equation 3.1 from Tables 3.1 and 3.2, the rolling friction (Frr) was calculated to be 66N. Subsequently, applying Equation 3.2 determined the amount of power needed to overcome this 66N force at 65 km/h and 8^0, resulting in a value of 1.19 KW.

.

$$P_{rr} = F_{rr} * V(m/s) \tag{3.2}$$

where P_{rr} is the power to overcome rolling friction and V is the car speed.

Slope Resistance

Slope resistance is the impact of gravity that a vehicle experiences when it's on an incline. It opposes motion uphill and assists motion downhill. When analyzing vehicle performance, uphill driving conditions are considered. The angle between the road and the horizontal, denoted by θ (Chauhan, 2015; Mehrdad et al., 2005), is used to calculate the slope resistance force acting on the vehicle:

$$F_g = W \sin\theta \tag{3.3}$$

where F_g is the slope resistance force. The calculated slope resistance force is 928.4N.

To overcome this 928.4N slope resistance force at speeds of 20 km/h and 8^0, a climbing power of 5.16 KW is required, as determined by Equation 3.4.

$$P_g = F_g * V_c \left(m/s \right) \tag{3.4}$$

where P_g is the climbing force and V_c is the climbing velocity.

Aerodynamic Drag Force

A vehicle encounters wind resistance, which opposes its motion when driving against the wind and aids it when driving with the wind. This aerodynamic drag is comprised of two primary components (Mehrdad et al., 2005): shape drag, determined by the vehicle's overall shape, and skin friction resulting from air flowing over the vehicle's surface.

Shape drag: As a vehicle moves forward, it compresses the air in front, creating a region of high pressure. Simultaneously, Because the air cannot quickly fill the empty space behind the car, a low-pressure area develops. This pressure differential generates a force opposing the vehicle's motion, known as shape drag, which is influenced primarily by the vehicle's aerodynamic design.

Skin friction drag: arises from the air's resistance as it moves across the vehicle's surface. The air in direct contact with the vehicle moves at a similar speed, while the air further away remains relatively stationary. This velocity difference between the air layers creates frictional forces, contributing to the overall aerodynamic drag.

$$F_{ad} = \frac{1}{2} \rho A_d C_d V^2 \tag{3.5}$$

where A_d is the frontal projected area(m^2), ρ is the air density(kg/m^3) and C_d is the drag coefficient (typically, 0.2 to 0.4, with 0.3 for passenger cars and 0.4 for common sports utility vehicles) (Nam, 2018). Based on these parameters, the calculated aerodynamic drag force is 82.6 N.

Aerodynamic forces were plotted for vehicle speeds ranging between 0 to 65 km/h (0 to 18 m/s), assuming stationary air. Figure 3.4 illustrates these forces.

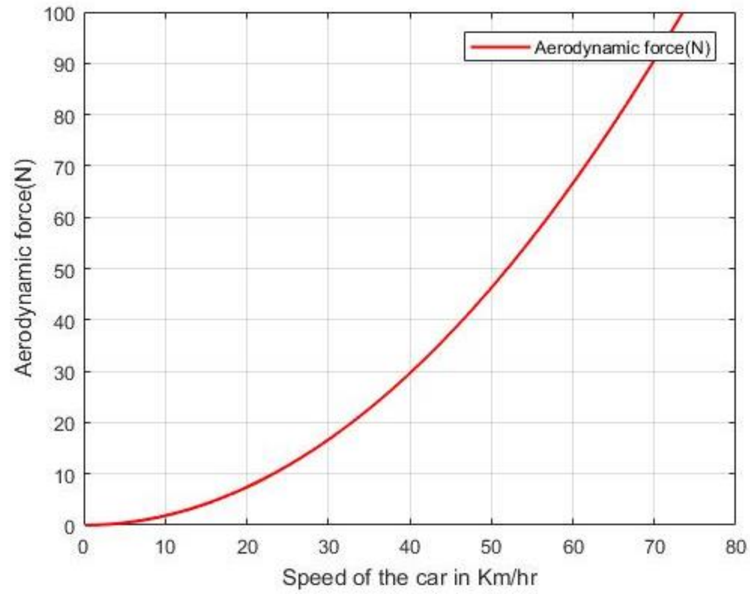

Figure 3.4: Aerodynamic Drag Force vs. Vehicle Speed (km/hr)

At 65 km/h, aerodynamic drag force must be resisted with a power output of 1.49 kW.

$$P_{ad} = F_{ad} * V(m/s) \tag{3.6}$$

where P_{ad} the aerodynamic drag power and F_{ad} is the aerodynamic drag force. Figure 3.5 illustrates the total motive force needed for every part of the vehicle while climbing a hill at a steady 20 km/h in still air conditions.

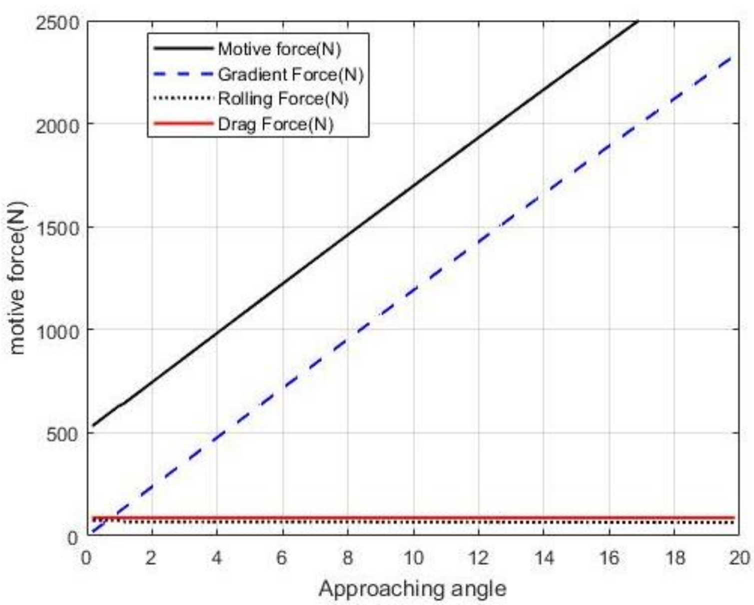

Figure 3.5: Motive Force vs. Vehicle Approach Angle

The rolling resistance coefficients for various road surface types summarizes in Table 3.1 (Chauhan, 2015)

Table 3.1: Rolling resistance co-efficient values (Chauhan, 2015)

Contact Surface	C_{rr}
Concrete (good/ fair/ poor)	0.010/ 0.015/ 0.020
Asphalt (good/ fair/ poor)	0.012/ 0.017/ 0.022
Macadam (good/ fair/ poor)	0.015/ 0.022/0.037
Snow (2 inch/ 4 inch)	0.025/0.037
Dirt (smooth/ sandy)	0.025/ 0.037
Mud (firm/ medium/ soft)	0.037/ 0.090/ 0.150
Grass (firm/ soft)	0.055/ 0.075
Sand (firm/ soft/ dune)	0.060/ 0.150/ 0.300

In the absence of a slope, as on a straight road, no slope force acts on the vehicle. Figure 3.6 depicts the total motive force considering all acting forces. The vehicle is assumed to travel straight at an average speed between 0 and 65 km/h with the vehicle's acceleration is 0.5 m/s^2. The road surface exhibits a kinetic friction coefficient of 0.01 and a static friction coefficient of 0.1.

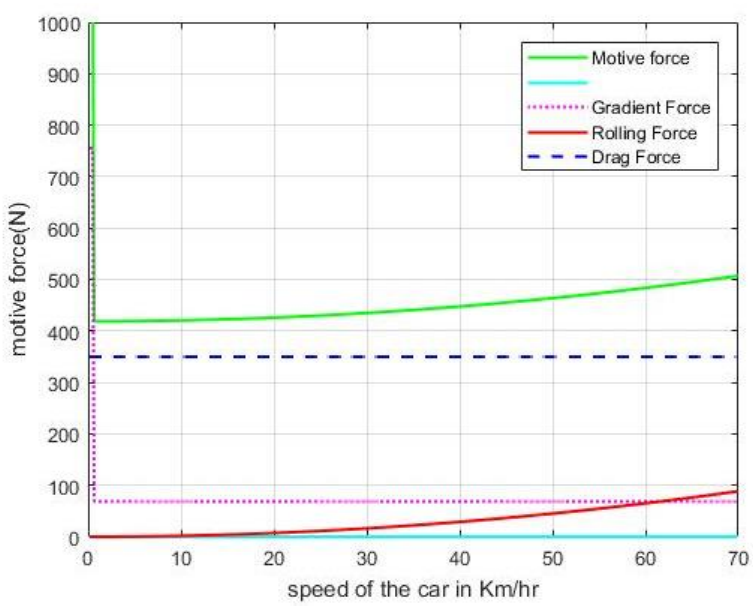

Figure 3.6: Motive Force (N) vs. Vehicle Speed (km/h)

By analyzing Equations 3.1 to 3.6, the maximum power demand from the PMSM to propel the vehicle under various driving conditions can be determined. Consequently, the peak tractive force and power needed for vehicle propulsion can be calculated.

The total acting force on the vehicle:

$$F_t = F_{rr} = F_g + F_{ad} \tag{3.7}$$

The maximum power:

$$P_{t(\max)} = P_{rr} + P_g + P_{ad} \tag{3.8}$$

The total force 1077 N and the total power could be 7.84 KW. However, a motor power rating of 7.84 kW is insufficient due to power losses incurred during transmission to the wheels. To account for these losses, the required mechanical power output for propelling the vehicle can be calculated as follows:

$$P_{M\,(\max)} = \frac{P_{t(\max)}}{\eta} \tag{3.9}$$

where η (0.98) is efficiency of transmission gear, $P_{M(\max)}$ is the vehicle requires a mechanical power output of 8 KW and $P_{t(\max)}$ is the maximum power for the PMSM. When the fully loaded vehicle climbs a steepest inclination of 8-degrees at a speed of 20-km/h, the maximum tractive power is needed. To make up for the battery's and motor's decreased power availability, it is necessary to decrease vehicle speed to increase torque.

Weight and cost will go up with larger batteries and motors with higher power ratings. The motor power needed to keep moving at a steady 20 km/h across different approach angles is illustrates in Figure 3.7.

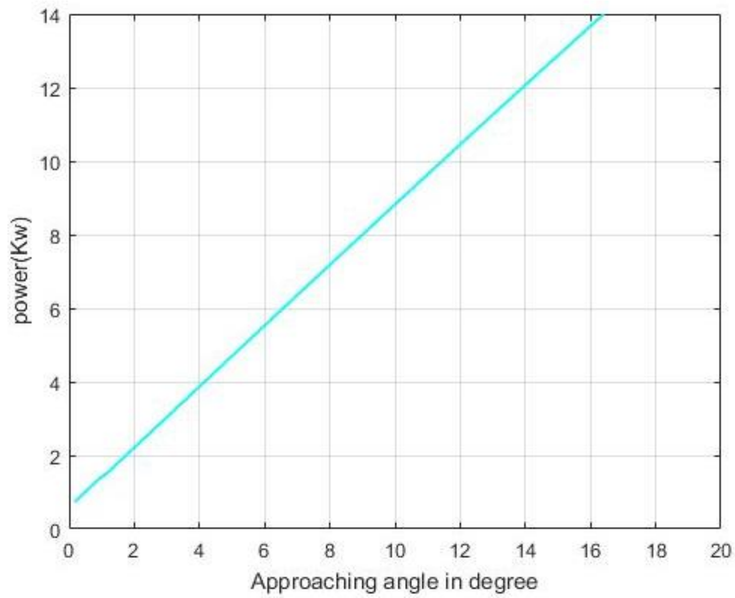

Figure 3.7: Motor Power Consumption vs. Approach Angle

Figure 3.7 depicts the motor power needed when a vehicle traveling at a constant 20 km/h suddenly encounters an incline with a specific approach angle. The maximum achievable approach angle at 20 km/h is 8 degrees, requiring 8 kW of power. As vehicle speed increases, so does power consumption. Therefore, determining the maximum and rated power for the specified loaded vehicle is crucial to meet speed and torque demands.

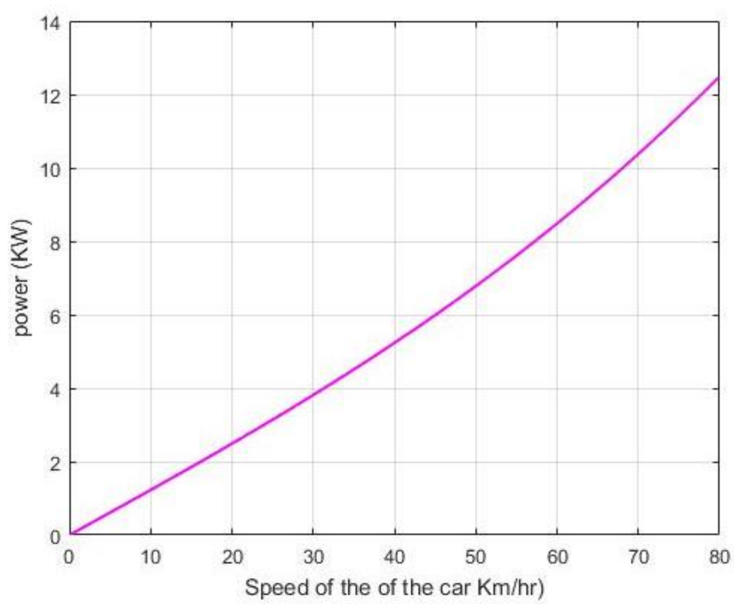

Figure 3.8: Consumed Power (kW) vs. Vehicle Speed(km/h)

A fully loaded vehicle accelerates from rest at 0.5 m/s^2 on a linear street. Figure 3.8 illustrates the speed of the vehicle in respect to power consumption. Based on the figure, the vehicle achieves a top speed of 80 km/h and an 8-kW power output. To accurately model the system, determining the motor's rated and maximum torque requirements is essential. Once the motor's necessary power output is established, the gear system can adjust torque and speed accordingly.

3.5.2 Selection of the Required Torque for the Drive Wheel

To ensure optimal performance, the drive motor must deliver the necessary torque to the drive wheel. This torque can be calculated using two methods, considering the vehicle's mass (680 kg), desired velocity (18.055 m/s), angular velocity (157 rad/s), wheel radius (0.2 m), and required power (8 kW).

$$T_{ideal} = \frac{P_{M\,(\max)}}{\omega_r} \tag{3.10}$$

$$T_{ideal} = \frac{8Kw}{157 rad / s} = 50.95 Nm$$

Overall transmission efficiency (η) of EV is considered.

$$T_{Actual} = T_{ideal} * \eta$$

$$\omega_{Wheel} = \frac{V}{r} \tag{3.11}$$

$$Gear\_Ratio(G) = \frac{\omega_r}{\omega_{Wheel}}$$

$$T_{Wheel} = T_{ideal} * G$$

$$T_{Actual} = 50.95 * 0.89 = 45.35 Nm$$

$$\omega_{Wheel} = \frac{18.055\, m/s}{0.2m} = 90.28\, rad/\sec$$

$$Gear\_Ratio(G) = \frac{157\, rad/s}{90.28\, rad/s} = 1.73$$

$$T_{Wheel} = 45.35 * 1.73 = 88.14 Nm$$

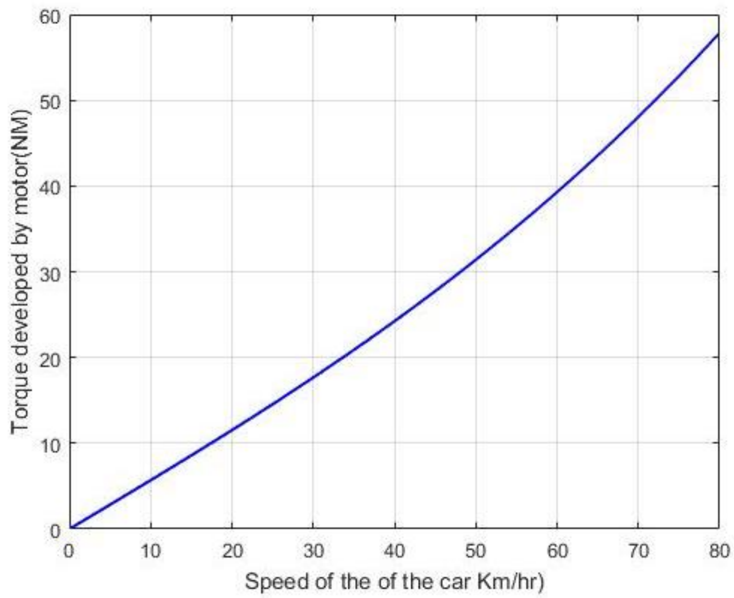

Figure 3.9: Motor torque(Nm) vs. Vehicle Speed(km/h)

3.5.3. Electric Bajaj (3-wheeler) Specification and Traction Selection

The technical specifications of the three-wheel Bajaj vehicle are detailed in Table 3.2 (Vidhya & Mahadevan, 2019). Additionally, Table 3.3 provides a full breakdown of the PMSM's particular parameters (Liuping et al., 2015).

Table 3.2: Technical Specification of three-wheel Bajaj (Vidhya & Mahadevan, 2019)

Parameter	Value [unit]
Gross Vehicle Mass (Vehicle + payload weight)	680 Kg (350 + 330) Kg
Gravitational acceleration, g	9.81 kg/m^2
Angle of inclination, θ	8^0
Maximum speed, V	65 Km/hr
Climbing Velocity, V_c	20 Km/hr
Co-efficient of rolling friction, C_{rr}	0.01
Density of air, ρ	1.22 kg/m^3
Frontal area, A_d	2.09 m^2
Co-efficient Drag, C_d	0.2
Transmission efficiency, η	0.98

Based on previous calculations and vehicle data from the Bajaj RE three-wheeler EV, a PMSM has been chosen as the as the driving motor in the Bajaj three-wheeler electric vehicle. Table 3.3 provides a full breakdown of the PMSM's particular parameters. (Liuping et al., 2015).

Table 3.3: The PMSM parameter specification utilized in this dissertation (Liuping et al., 2015)

Description	Symbol	Value
Stator resistance	Rs	2.875 Ω
Pole	P	4
Efficiency	η	98 % @ rated value
Rotor moment of inertia	J	0.0008 kg.m^2
Frequency	f	50 Hz
Voltage	V	300 V
Inductance	L_d and L_q	0.0085 H and 0.0085 H
Rated torque	T_{rated}	45 Nm
Viscous friction	B	1.1e-4Nm.s
Rated Power	Prated	8kW
Flux linkage due to Permanent magnet	λ_m	0.175Wb
Rated speed	ω_{rated}	1500 rpm
Rated current	I_{rated}	2.9A

3.6 PMSM Mathematical Modeling

Controlling a PMSM in a three-phase system is complex due to its nonlinear, multivariable, and coupled nature. To address these challenges, this study employs vector control. This method simplifies the complex PMSM model into a more manageable DC motor-like equivalent through coordinate transformations. Specifically, Clark and Park transformations, along with their inverses, are utilized (Ren et al., 2020).

Coordinate transformations linearize the intricate three-phase PMSM model, facilitating analysis and control. By converting the system into a linear equivalent, control system design becomes more straightforward, enabling the implementation of advanced control strategies. This established technique enhances PMSM drive performance and reliability.

3.6.1 Transformations

Complex voltage equations and inductances describe the behavior of three-phase AC devices. To simplify analysis, coordinate transformations are employed. Field-Oriented Control (FOC) utilizes multiple reference frames connected by Clark and Park transformations. These transformations are essential for controlling both PMSMs and induction devices. By simplifying the complex voltage equations, these transformations facilitate a deeper understanding of machine characteristics (Maji et al., 2015; Zambada & Deb, 2010).

The FOC of PMSM deals with three reference frames (Deo & Shekokar, 2015):

1. Three-phase (a-b-c) stator reference frame: the three phases stator (a-b-c) are distributed equally around the stator, with a 120-degree electrical phase difference between them.
2. Two-phase (α-β) stationary reference frame: The three-phase system is mathematically converted in-to two phase system utilizing this frame. The α and β axes are stationary and orthogonal.
3. Two-phase rotating reference frame (d-q): This frame is also a mathematical transformation. The q-axis is perpendicular to the rotor's magnetic field, whereas the d-axis is in accordance with it. The rotor rotates at the same speed as the d and q axes.

Figure 3.10 visually depicts the relationships and transformations between the three reference frames: (a, b, c), (α, β), and (d-q).

Clarke Transformation

Three phase quantities can be simplified into a two-phase representation using a mathematical method called the Clarke transformation.

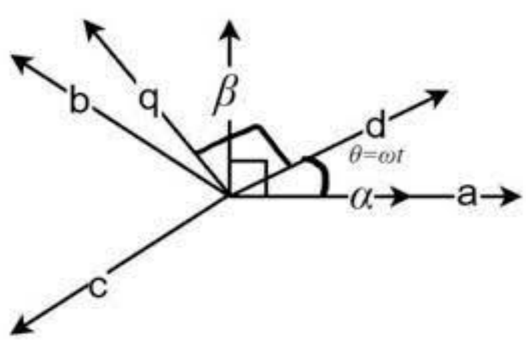

Figure 3.10 Combined reference frame.

As shown in Figure 3.11, the Clarke transformation converts three phase quantities from the a- b-c reference frame into the two phase α-β stationary reference frame.

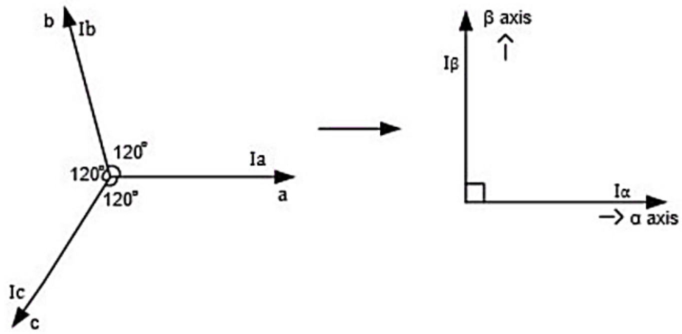

Figure 3.11 Clarke Transformation

The equations below define the Clarke transformation.:

$$\begin{aligned} f_\alpha &= f_a + f_b \cos(120) + f_c \cos(240) \\ f_\beta &= 0 + f_b \sin(120) + f_c \sin(240) \end{aligned} \tag{3.12}$$

where f used for current and voltage

$$\begin{aligned} i_\alpha &= K(i_a - \frac{1}{2} i_b - \frac{1}{2} i_c) \\ i_\beta &= K(\frac{\sqrt{3}}{2} i_b - \frac{\sqrt{3}}{2} i_c) \end{aligned} \tag{3.13}$$

where $i_a + i_b + i_c = 0$ and the recommended K values is $K= 3/2$

In matrix form

$$\begin{bmatrix} i_\alpha \\ i_\beta \end{bmatrix} = \frac{3}{2} \begin{bmatrix} 1 & -\frac{1}{2} & -\frac{1}{2} \\ 0 & \frac{\sqrt{3}}{2} & -\frac{\sqrt{3}}{2} \end{bmatrix} \begin{bmatrix} i_a \\ i_b \\ i_c \end{bmatrix} \tag{3.14}$$

Park Transformation

The Park transformation can be utilized to convert the α-β numbers into a rotating d-q reference frame, as demonstrated in Figure 3.12.

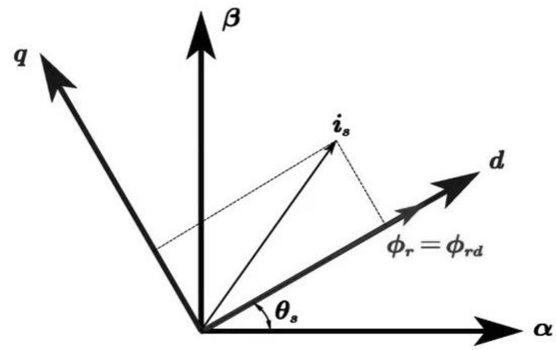

Figure 3.12: The Park Transformation

The following equations define the Park transformation:

$$\begin{bmatrix} i_d \\ i_q \end{bmatrix} = \begin{bmatrix} \cos\phi & \sin\phi \\ -\sin\phi & \cos\phi \end{bmatrix} \begin{bmatrix} i_\alpha \\ i_\beta \end{bmatrix} \tag{3.15}$$

where i_d and i_q is the current components in the d and q-reference frame, i_α and i_β is the current components in the α and β reference frame and ϕ is the electrical rotor angle.

Inverse Park Transformation

As illustrated in Figure 3.12, the inverse Park transformation returns quantities from the revolving d-q reference frame to the stationary α-β reference frame. The following equations define the transformation:

$$\begin{bmatrix} i_\alpha \\ i_\beta \end{bmatrix} = \begin{bmatrix} \cos\phi & -\sin\phi \\ \sin\phi & \cos\phi \end{bmatrix} \begin{bmatrix} i_d \\ i_q \end{bmatrix} \tag{3.16}$$

3.6.2 The a-b-c reference frame's PMSM model

In the a- b- c reference frame, the motor's voltage equation is written as (Suman & Mathew, 2018):

$$V_{abc} = R' i_{abc} + \frac{\partial \lambda_{abc}}{\partial t} \tag{3.17}$$

where R is the stator resistance, λ_{abc} is the stator flux linkages in a- b- c phases, i_{abc} is the three phase currents, and V_{abc} is three phase stator voltages.

$$(f_{abc})^T = [f_a, f_b, f_c] \tag{3.18}$$

Where f can represent V, I, or λ.

$$R^{'} = \begin{bmatrix} R & 0 & 0 \\ 0 & R & 0 \\ 0 & 0 & R \end{bmatrix} \tag{3.19}$$

The equation for flux linkage is expressed by:

$$\lambda_{abc} = L \times \begin{bmatrix} i_a \\ i_b \\ i_c \end{bmatrix} + \lambda_m \begin{bmatrix} \sin(\theta) \\ \sin(\theta - \frac{2\pi}{3}) \\ \sin(\theta + \frac{2\pi}{3}) \end{bmatrix} \tag{3.20}$$

From Equation (3.20):

$$\begin{aligned} \lambda_a &= Li_a + \lambda_m \sin(\theta) \\ \lambda_b &= Li_b + \lambda_m \sin(\theta - \frac{2\pi}{3}) \\ \lambda_c &= Li_c + \lambda_m \sin(\theta + \frac{2\pi}{3}) \end{aligned} \tag{3.21}$$

where L is the inductance, λ_m is the flux linkage and E is back EMF in the representative phases

The electromagnetic torque turns in to (Suman & Mathew, 2018):

$$T_e = (E_a i_a + E_b i_b + E_c i_c)/\omega \tag{3.22}$$

Then it can be written as:

$$T_e = P/2\lambda_m[(i_a - 1/2 i_b - 1/2 i_c)\sin(\theta) - \sqrt{3}/2(i_b - i_c)\cos(\theta)] \tag{3.23}$$

where P is the number of poles

3.6.3 Motor Model in (d-q) Reference Frame

For analysis and control, the PMSM's d-q axis model offers a condensed representation. The intricate three phase system is simplified in-to a two axis rotating reference frame to create this model. The following are the voltage equations expressed in d-q coordinates (Suman & Mathew, 2018):

$$V_d = Ri_d + \frac{d\lambda_d}{dt} - \omega_r \lambda_q$$
$$V_q = Ri_q + \frac{d\lambda_q}{dt} + \omega_r \lambda_d \tag{3.24}$$

where i_d and i_q are d and q axis currents, V_d and V_q are d and q axis voltages, respectively, R is the stator resistance, L_d and L_q is d and q axis inductance values, and λ_d and λ_q are d and q axis flux linkages given as:

$$\lambda_d = L_d i_d + \lambda_m \tag{3.25}$$

$$\lambda_q = L_q i_q \tag{3.26}$$

Substituting the values of λ_d and λ_q into the previous equations and rearranging, we obtain:

$$V_d = Ri_d - \omega_r L_q i_q + \frac{d}{dt}(L_d i_d + \lambda_m)$$
$$V_q = Ri_q + \omega_r (L_d i_d + \lambda_m) + L_q \frac{di_q}{dt} \tag{3.27}$$

Based on the derived formulas, the following differential equations for the currents can be obtained:

$$\frac{di_d}{dt} = -\frac{R}{L_d} i_d + \omega_r \frac{L_q}{L_d} i_q + \frac{V_d}{L_d}$$
$$\frac{di_q}{dt} = -\frac{R}{L_q} i_q - \omega_r \frac{L_d}{L_q} i_d - \omega_r \frac{\lambda_m}{L_q} + \frac{V_q}{L_q} \tag{3.28}$$

Electromagnetic torque is given by:

$$T_e = \frac{3P}{2}(\lambda_d i_q - \lambda_q i_d) \tag{3.29}$$

To achieve maximum torque, minimize torque ripple, and mitigate reluctance effects, vector control is employed. Zeroing the d-axis current causes the stator current vector aligns with the q-axis, resulting in optimal torque production. The torque equation under these conditions is (Sharifian et al., 2009):

$$T_e = \frac{3P}{2}\lambda_m i_q \tag{3.30}$$

Therefore, the only way to modify torque is to adjust the q-axis current (i_q). In any frame of reference, the electromagnetic torque is defined as:

$$J\frac{d\omega_r}{dt} = T_e - B\omega - T_m; \quad \text{where } \omega_r = \frac{d\theta_r}{dt} \tag{3.31}$$

Thus, from Equations (3.30) and (3.31)

$$\frac{d\omega_r}{dt} = \frac{1}{J}\left(\frac{3P}{2}\lambda_m i_q - B\omega_r - T_m\right) \tag{3.32}$$

Set of Equation (3.30) and $\frac{d\theta}{dt} = \omega$, The PMSM's state equation is defined as:

$$\begin{bmatrix} \frac{di_d}{dt} \\ \frac{di_q}{dt} \\ \frac{d\theta}{dt} \end{bmatrix} = \begin{bmatrix} -\frac{R}{L}i_d + \omega i_q + \frac{V_d}{L} \\ -\frac{R}{L}i_q - \omega i_d - \frac{\lambda_m}{L}\omega + \frac{V_q}{L} \\ \omega \end{bmatrix} \tag{3.33}$$

Using Equations (3.25 and (3.26) $\omega = P\omega_r$ and $\theta = P\theta_r$, and

For the PMSM's mechanical motion, the state equation is:

$$\begin{bmatrix} \frac{d\theta}{dt} \\ \frac{d\omega_r}{dt} \\ \frac{di_d}{dt} \\ \frac{di_q}{dt} \end{bmatrix} = \begin{bmatrix} \omega \\ \frac{3P}{2}\lambda_m i_q - \frac{B}{J}\omega_r - \frac{T_l}{J} \\ -\frac{R}{L}i_d + P\omega_r i_q + \frac{V_d}{L} \\ -\frac{R}{L}i_q - P\omega_r i_d - P\frac{\lambda_m}{L}\omega_r + \frac{V_q}{L} \end{bmatrix} \tag{3.34}$$

where, V_d, V_q, i_d *and* i_q are d-coordinate and q-coordinate voltage and current component.

Equation (3.28) indicates that the PMSM is a complex system with time-varying behavior, coupling between variables, and nonlinearity.

Considering i_d, i_q, ω_r, and θ_r as state variables, V_d and V_q as input variables, and i_d and i_q as output variables.

The system's state-space model when it is under load is:

$$\begin{aligned} \dot{\boldsymbol{x}} &= \boldsymbol{Ax} + \boldsymbol{Bu} \\ y &= \boldsymbol{Cx} \end{aligned} \tag{3.35a}$$

where the state vector is x, output vector is y, control input vector is u and A, B and C matrices are defined as:

$$\boldsymbol{x} = \begin{bmatrix} i_d \\ i_q \\ \omega_r \\ \theta_r \end{bmatrix}, \boldsymbol{y} = \begin{bmatrix} i_d \\ i_q \end{bmatrix}, \boldsymbol{u} = \begin{bmatrix} V_d \\ V_q \end{bmatrix} \tag{3.36b}$$

$$\boldsymbol{A} = \begin{bmatrix} -\frac{R}{L_d} & \frac{L_q}{L_d}\omega_r & 0 & 0 \\ -\frac{L_d}{L_q}\omega_r & -\frac{R}{L_q} & -\frac{\lambda_m}{L_q} & 0 \\ 0 & \frac{3P}{2J}\lambda_m & -\frac{B}{J} & 0 \\ 0 & 0 & 1 & 0 \end{bmatrix}, \quad \boldsymbol{B} = \begin{bmatrix} \frac{1}{L_d} & 0 \\ 0 & \frac{1}{L_q} \\ 0 & 0 \\ 0 & 0 \end{bmatrix}, \quad \boldsymbol{C} = \begin{bmatrix} 1 & 0 & 0 & 0 \\ 0 & 1 & 0 & 0 \end{bmatrix} \tag{3.37c}$$

3.7 Voltage Source Inverters

To achieve variable speed operation, PMSM motors require a variable frequency AC power supply. As most vehicles utilize DC batteries, a power electronic converter, It is important to use a voltage source inverter that operates on three phases. By utilizing six gate signals produced by SVPWM, this inverter's semiconductor switches are controlled to generate the necessary variable frequency AC voltage (Colak et al., 2011; Rodriguez et al., 2007). Figure 3.13 shows a diagram displaying this three phase VSI (Boby & Kottalil, 2013).

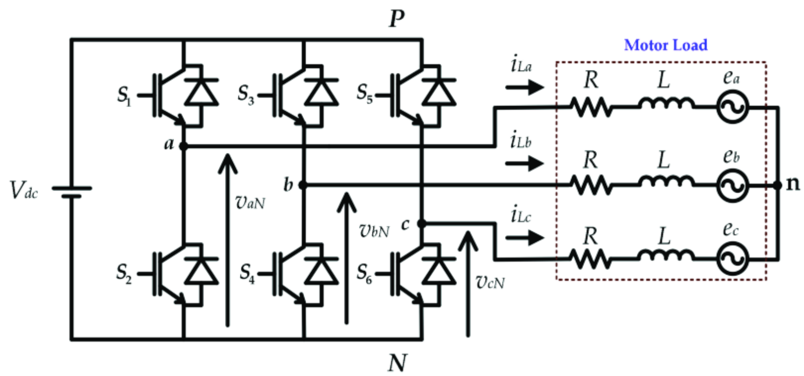

Figure 3.13: Three-phase Inverter

3.8 Space Vector Pulse Width Modulation (SVPWM)

An advanced approach to generating PWM signals in three phase inverters is called space vector modulation. Compared to traditional PWM methods, SVM offers superior performance by producing output voltages with higher fundamental components and lower harmonic distortion. Any modulation technique's main objective is to offer a changing output voltage with low harmonic distortion as possible, and SVM excels in achieving this objective for variable frequency drive applications (Kumar et al., 2010; Liang et al., 2014).

The three phase voltage equations are converted in-to the two-phase stationary α-β reference frame for Space Vector PWM, is demonstrated in Figure 3.14.

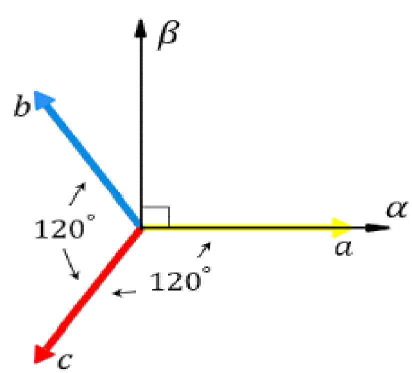

Figure 3.14. The α-β and a-b-c reference frames' relationship:

Equation 3.36 defines the mathematical link among the α-β and a- b- c reference frames, as seen in Figure 3.14.

$$f_{\alpha\beta 0} = K_s f_{abc} \tag{3.38}$$

where K_s is given below:

$$K_s = \frac{2}{3}\begin{bmatrix} 1 & -1/2 & -1/2 \\ 0 & \sqrt{3}/2 & -\sqrt{3}/2 \\ 1/2 & 1/2 & 1/2 \end{bmatrix} \tag{3.39}$$

The conversion from the a-b-c reference frame to the α-β reference frame can be visualized as projecting the three-phase vector onto a two dimensional plane oblique to the equal magnitude vector $(1\ 1\ 1)^T$. This projection results in six non-zero voltage vectors (V_1-V_6) and two zero vectors (V_0 and V_7).

The six non-zero voltage vectors form a hexagon, as illustrated in Figure 3.15. These vectors, along with two zero vectors, are evenly spaced at 60-degree intervals. These eight vectors collectively represent the possible switching states of the inverter and are symbolized by V_0(000), V_1(100), V_2(110), V_3(010), V_4(011), V_5(001), V_6(101), and V_7(111).

The reference voltage vector, V_{ref}, in the α-β plane is obtained by applying the same transformation to the desired output voltage. The fundamental idea behind Space Vector PWM (SVPWM) is to use a combination of the eight available switching states over a predetermined sampling period T to approximate this reference vector V_{ref}.

The diagram below shows the voltage space vectors for a three phase Voltage Source Inverter (VSI). The sectors in the d-q frame of reference are defined by the six no-zero voltage vectors, V_1 through V_6, which together span an angle of 60 degrees (Boby & Kottalil, 2013).

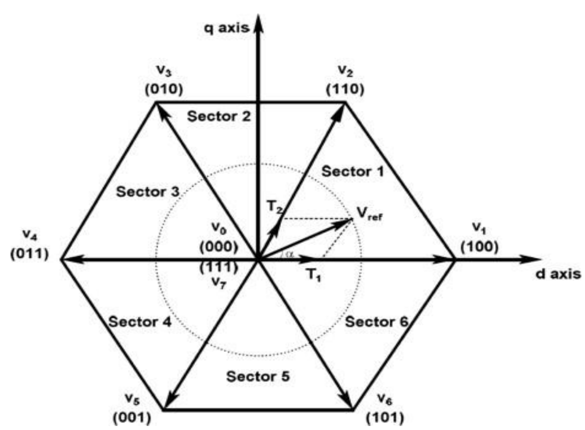

Figure 3.15: Space Vector diagram of (VSI)

Switching States

The output voltage vectors corresponding to switching states are listed below (Kumar et al., 2010).

Table 3.4**:** Inverter Switching States and Output Vectors

Voltage vector	Switching vector			Line to neutral Voltage			Line to line voltage		
	a	b	c	V_{an}	V_{bn}	V_{cn}	V_{ab}	V_{bc}	V_{ac}
V0	0	0	0	0	0	0	0	0	0
V1	1	0	0	2/3	-1/3	-1/3	1	0	-1
V2	1	1	0	1/3	1/3	-2/3	0	1	-1
V3	0	1	0	-1/3	2/3	-1/3	-1	1	0
V4	0	1	1	-2/3	1/3	1/3	-1	0	1
V5	0	0	1	-1/3	-1/3	2/3	0	-1	1
V6	1	0	1	1/3	-2/3	1/3	1	-1	0
V7	1	1	1	0	0	0	1	0	0

Note that it is necessary to multiply the corresponding voltage levels by V_{dc}.

Procedure implement SVPWM

Space Vector PWM implementation involves the following steps:

1. **Determine reference values:** Calculate V_q, V_d, V_{ref}, and the angle of a sector (α).
2. **Calculate duty cycles:** Based on the sector and reference vector, calculate the times T0, T1, and T2.
3. **Determine switching times:** Calculate the exact switching instants for each transistor (S1 to S6) based on the calculated duty cycles.

Step-1: Calculate angle(α), V_α, V_β, and V_{ref}.

The α-β frame is used by SVPWM and the Clarke transformation is applied, as opposed to the a-b- c reference frame. Hence, V_α and V_β are supplied as input to SVPWM. This voltage was calculated using the formula below:

$$\begin{bmatrix} V_\alpha \\ V_\beta \end{bmatrix} = \frac{2}{3} \begin{bmatrix} 1 & -\frac{1}{2} & -\frac{1}{2} \\ 0 & \frac{\sqrt{3}}{2} & -\frac{\sqrt{3}}{2} \end{bmatrix} \begin{bmatrix} V_{an} \\ V_{bn} \\ V_{cn} \end{bmatrix} \tag{3.40}$$

We can quickly ascertain the reference voltage (V_{ref}) and angle α as follows after determining V_α and V_β.

$$\begin{aligned} \left|V_{ref}\right| &= \sqrt{V_\alpha^{\ 2} + V_\beta^{\ 2}} \\ \alpha &= \tan^{-1}\left(\frac{V_\beta}{V_\alpha}\right) \end{aligned} \tag{3.41}$$

Step 2: Determine how long T_1, T_2, and T_0 will last.

The inverter switches' on-time lengths are represented by the time intervals T_1, T_2, and T_0. These timings can be calculated for Sector 1 as follows:

$$\begin{aligned} &\int_0^{Ts} \overline{V}_{ref} = \int_0^{T1} \overline{V}_1 dt + \int_{T1}^{T1+T2} \overline{V}_2 dt + \int_{T1+T2}^{Ts} \overline{V}_0 \\ &\Rightarrow T_s.\overline{V}_{ref} \cdot \begin{bmatrix} \cos(\alpha) \\ \sin(\alpha) \end{bmatrix} = T_1 . \frac{2}{3} . V_{dc} \cdot \begin{bmatrix} 1 \\ 0 \end{bmatrix} + T_2 . \frac{2}{3} . V_{dc} \cdot \begin{bmatrix} \cos\left(\frac{\pi}{3}\right) \\ \sin\left(\frac{\pi}{3}\right) \end{bmatrix} \end{aligned} \tag{3.42}$$

$$T_2 = T_s . \alpha . \frac{\sin(\alpha)}{\sin\left(\frac{\pi}{3}\right)} \tag{3.43}$$

$$T_1 = T_s . \alpha . \frac{\sin\left(\frac{\pi}{3} - \alpha\right)}{\sin\left(\frac{\pi}{3}\right)} \quad \text{(where, } 0 \le \alpha \ge 60^0\text{)} \tag{3.44}$$

where Ts and α are total switching time and modulation index which are presented in following equation:

$$T_s = \frac{1}{f_s} \quad \text{and} \quad a = \frac{\left|\bar{V}_{ref}\right|}{\frac{2}{3}.V_{dc}} \tag{3.45}$$

The switching times T_1 and T_2 for any sector can be determined by applying the subsequent equations:

$$\begin{aligned} T_1 &= \frac{\sqrt{3}.T_z.\left|\bar{V}_{ref}\right|}{V_{dc}}.\sin\left(\frac{n}{3}\pi - \alpha\right) \\ T_2 &= \frac{\sqrt{3}.T_z.\left|\bar{V}_{ref}\right|}{V_{dc}}.\left(\sin\left(\alpha - \frac{n-1}{3}\pi\right)\right) \end{aligned} \tag{3.46}$$

where n is the sector, which ranges from 1 to 6.

$T0$ is determined as:

$$T_0 = T_s - (T_1 + T_2) \tag{3.47}$$

Step 3 Find out when each transistor switches on and off.

The bottom switch of the inverter is off while the equivalent upper switch is on, and vice versa. This is how the switches work together complimentary. The specific switching times for each transistor within a given sector are detailed in the table below (Kumar et al., 2010):

Table 3.5: Calculating the switching time in every sector

Sector number (n)	Upper Switches (S_1, S_3, S_5)	Lower Switches (S_2, S_4 S_6)
1	$S_1=T_1+T_2+T_0/2$ $S_3=T_2+T_0/2$ $S_5=T_0/2$	$S_4=T_0/2$ $S_6=T_1+T_0/2$ $S_2=T_1+T_2+T_0/2$
2	$S_1=T_1+T_0/2$ $S_3=T_1+T_2+T_0/2$ $S_5=T_0/2$	$S_4= T_2+T_0/2$ $S_6=T_0/2$ $S_2=T_1+T_2+T_0/2$
3	$S_1= T_0/2$ $S_3=T_1+T_2+T_0/2$ $S_5=T_2+T_0/2$	$S_4= T_1+T_2+T_0/2$ $S_6=T_2+T_0/2$ $S_2=T_0/2$
4	$S_1= T_0/2$ $S_3=T_1+T_0/2$ $S_5= T_1+T_2+T_0/2$	$S_4= T_1+T_2+T_0/2$ $S_6=T_2+T_0/2$ $S_2= T_0/2$
5	$S_1=T_2+T_0/2$ $S_3=T_0/2$ $S_5= T_1+T_2+T_0/2$	$S_4= T_1+T_0/2$ $S_6=T_1+ T_2+T_0/2$ $S_2=T_0/2$
6	$S_1=T_1+T_2+T_0/2$ $S_2=T_0/2$ $S_3=T_1+T_0/2$	$S_1= T_0/2$ $S_2= T_1+T_2+T_0/2$ $S_3=T_2+T_0/2$

CHAPTER FOUR

CONTROLLER DESIGN

This chapter investigates the employment of a cascaded control mechanism to control a Permanent Magnet Synchronous Motor (PMSM). An integral-sliding mode controller with exponential reaching law (ISMC-ERL) regulates motor speed in the outer loop, while two PI controllers manage the inner current loop. The electromagnetic torque is primarily determined by the quadrature current (i_q), while the inner loop manages the d-q axis currents ((i_d and i_q).

Effective control system design is crucial for electric motors in applications like electric vehicles. The primary goal is to maintain precise and stable motor speed across a wide operating range while mitigating the effects of disturbances and load variations. While PI controllers offer simplicity, their performance limitations can be pronounced in complex systems like electric vehicles, especially under dynamic conditions.

In such applications, more advanced controllers are necessary to handle the nonlinearities and achieve superior dynamic performance. Sliding Mode Control (SMC) stands out as a promising option due to its robustness against disturbances and ability to mitigate chattering, a common issue in traditional SMC implementations. Chattering-free SMC variants are particularly attractive for achieving stable and efficient motor control in demanding environments like electric vehicles.

4.1 Design of the Current Controller's (Inner Loop Control)

PI controller is employed for inner loop of the PMSM to control the current with the aim of improving the error among measured and desired current $i_{d\text{-}q}$. The gain parameters are tuned by using.

$$u_d = K_{p1}(i_{dref} - i_d) + K_{i1}\int(i_{dref} - i_d)dt \tag{4.1}$$

$$u_q = K_{p2}(i_{qref} - i_q) + K_{i2}\int(i_{qref} - i_q)dt \tag{4.2}$$

where i_{dref} and i_{qref} are the reference values for stator current in the d and q axis, respectively. K_{p1} and K_{p2} are the proportional gains and K_{i1} and K_{i2} are the integral gains.

4.2 Design of the PID Controller for Comparison (Outer Loop Control)

PID controllers are quite common in motor drive systems because of their efficiency and ease of use. Approximately 90% of industrial controllers employ PID algorithms because of their ease of implementation and practical performance (Bennett, 1994; Wu et al., 2014).

A PID controller regulates a process by comparing the actual output to the desired output and adjusting the control signal accordingly. To reduce the difference over time, it continually modifies the control input depending on the derivative, integral, and proportional terms of the error.

PID Controller Parameters:

- **Proportional gain (*Kp*):** Used to enhance the transient response rise time and settling time
- **Integral gain (*Ki*):** Accounts for past errors and eliminates steady-state error.
- **Derivative gain (*Kd*):** Uses the error's rate of change to predict future trends in errors.

The PID controller algorithms are:

$$e(t) = r(t) - y(t) \tag{4.3}$$

$$u(t) = k_p e(t) + k_i \int e(t)\,dt + k_d \frac{de(t)}{dt} \tag{4.4}$$

$$u(t) = k_p \left\{ e(t) + \frac{1}{T_i} \int e(t) + T_d \frac{de(t)}{dt} \right\} \tag{4.5}$$

The Laplace transformation of PID controller output u(t) is calculated using:

$$u(t) = k_p \left\{ 1 + \frac{1}{s \cdot T_i} + s \cdot T_d \right\} \tag{4.6}$$

where *u(t)* is the PID controller's output, *r(t)* is the reference input, T_d is the derivative time constant, T_i is the integral time constant, *y(t)* is the system's output, and *e(t)* is the error signal among the reference input and system output.

4.3 Design of the Proposed Integral Sliding Mode Controller (Outer Loop Control)

Sliding Mode Control (SMC) is a nonlinear control approach that is widely recognized for its resilience to changes in system characteristics as well as outside influences. This characteristic sets it apart from other linear and nonlinear control techniques. Speed controllers for permanent magnet motors operating at high speeds must be able to respond quickly, track well, have less overshoot, and effectively reject disturbances.

Regarding SMC, there are two main benefits. Initially, the system's dynamic behavior can be tailored by selecting the sliding function correctly. This makes it possible to modify the system's response to satisfy particular performance requirements. Second, by making the closed-loop response relatively insensitive to specific kinds of uncertainties or disturbances, SMC provides robustness. SMC is especially beneficial in applications where it is necessary to efficiently manage external disturbances or uncertainty in the system dynamics due to its robustness

Traditionally, PI controllers were employed for motor speed control, but their performance was often hindered by poor tracking and a lack of robustness. To overcome these limitations, nonlinear and robust control strategies, such as sliding mode control, have been increasingly adopted in these applications.

To enhance the tracking performance, disturbance rejection, and mitigate chattering in traditional SMCs, various improvements have been explored. These include improving the design of sliding surfaces, applying reaching law techniques, using higher-order sliding mode controllers, and creating hybrid strategies that incorporate disturbance compensation or artificial intelligence (Mohd Zaihidee et al., 2019).

Designing a sliding mode controller involves two primary steps: defining a suitable sliding surface and developing a control input to drive the system onto this surface. Achieving and maintaining the sliding mode is crucial for ensuring system stability and robust performance (Mohd Zaihidee et al., 2019).

$$s\dot{s} < 0 \tag{4.7}$$

where s is the sliding surface.

Integral Sliding Mode Control (ISMC) was developed to impose sliding mode behavior right away on the system. This implies that matching uncertainties can be compensated for over the course of the system response by an ISMC-based controller.

ISMC assumes a pre-existing nominal plant with a designed state feedback controller ensuring Stability of closed loops and achieving performance objectives. A discontinuous controller is then added to maintain nominal performance while rejecting external disturbances. This approach allows for retrofitting ISMC onto existing controllers to address matched uncertainties. While sliding mode-based methods effectively handle matched uncertainties, unmatched uncertainties, those outside the input distribution matrix's range, remain unaddressed

To illustrate the design process, think of a linear time-invariant (LTI) system that is uncertain and is expressed by:

$$\dot{x}(t) = Ax(t) + Bu(t) + M\xi(t, x) + fu(t, x) \tag{4.8}$$

where $B \in IR^{n\times m}$, $A \in IR^{n\times n}$

Assumption 2.1: The controllability of the pair (A, B) is guaranteed when matrix B has full column rank (rank(B) = m) where $1 \leq m < n$.

Assumption 2.2: Assumed to be known, the matrix $M \in IR^{n\times l}$ is located within the subspace spanned by the columns of matrix B.

Under 2.1 and 2.2 assumptions, ξ (t, x) denotes an unidentified disruption that is bounded. Matrix M can be broken down as M = BD and satisfies the matching requirement for certain $D \in IR^{m\times l}$.

Assumption 2.3: Since the function $f_u(t, x)$ expresses unequalled ambiguity, it is not a member of matrix B's column space. It is assumed that this uncertainty is constrained to a known upper bound.

In relation to Equation (4.8), the nominal linear system is provided by:

$$\dot{x}(t) = Ax(t) + Bu_o(t) \tag{4.9}$$

where $u_0(t)$ is a nominal control rule that is created to produce the required nominal performance using any appropriate state feedback technique.

Given the controllability of the pair (A, B), state feedback controller of the form.

$$u_o(t) = -Fx(t) \tag{4.10}$$

where $x_0(t)$ is the nominal state trajectory and $F \in \mathbb{R}^{m\times n}$ is a state feedback gain intended to achieve desired performance for the nominal state trajectories of the system (Equation 4.9). Any appropriate state feedback design technique can be used to determine the matrix *F*.

The goal is to create a control law *u(t)* for which, under sliding mode, the state trajectories *x(t)* of Equation (4.8) exactly follow the nominal trajectories $x_0(t)$. This will only be possible if the initial circumstances are the same, that is, $x(0) = x_0$, and the unmatched uncertainty $f_u(.)$ is zero. To achieve this, the order of the sliding dynamics must match that of the nominal system (Hamayun et al., 2016).

4.3.1 Sliding function

The objective is to offer an appropriate control that guarantees reliable performance even when there are changes in parameters and load. Tracking a reference mechanical angular velocity ωref is necessary for the rotor mechanical angular velocity ω_r. An additional sliding manifold is suggested to monitor the mechanical angular velocity ωr and ensure that the error dynamics conforms to the intended second order dynamic. It is possible to achieve the following form by denoting ω_{ref} the desired velocity.

In Equation (4.11), the sliding surface is represented by s, the tracking error is illustrated by e, and the sliding surface coefficient is symbolized by c, a positive scalar.

$$s = e + c\int e(t)\,dt \tag{4.11}$$

$$e = \omega_{ref} - \omega_r \tag{4.12}$$

where *e(t)* is the error in speed, ω_r is the exact speed and ω_{ref} is the preferred speed.

The integral component eliminates the steady-state speed error commonly found in traditional PI controllers. Subsequently, a switching function based on the sliding surface, *s*, determines the motor's control input.

4.3.2 Design of an ISMC Law

In order to guarantee that the PMSM tracks the intended speed reference precisely, the ISMC forces the speed mistake to achieve and sustain sliding surface conditions.

Differentiate the sliding surface, s, constantly until the control input is explicitly included in the equation in order to handle load torque as an external disturbance.

$$\dot{e} = \dot{\omega}_{ref} - \dot{\omega}_r \tag{4.13}$$

$$\dot{e} = \dot{\omega}_{ref} - \left(\frac{3P}{2J} \lambda_m i_{qref} - \frac{B}{J} \omega_r - \frac{Tl}{J} \right) \tag{4.14}$$

Now the derivate of the sliding surface s equal to:

$$\dot{s} = \dot{e} + ce \tag{4.15}$$

$$\dot{s} = -\left(\frac{3P}{2J} \lambda_m i_q - \frac{B}{J} \omega_r - \frac{Tl}{J} \right) + c\left(\omega_{ref} - \omega_r \right) \tag{4.16}$$

To control the system, we employ an Exponential Reaching Law (ERL). This technique guarantees that the switching variable converges to the switching manifold, represented by the letter "*s*," at a constant rate determined by the constant "*ks*". The specific implementation is as follows (Bharathi et al., 2014):

$$\dot{s} = -\varepsilon \operatorname{sgn}\left(s \right) - ks \tag{4.17}$$

where: $\dot{s} = -ks$ is an exponential term, and its solution is $s = s(0)e^{-kt}$ .In the case of exponential reaching law, to guarantee faster convergence speed, especially when s is near to zero, the term $\dot{s} = -\varepsilon sign(s)$ is used. Moreover, to reduce chattering, we should design a bigger value of k and use a smaller value of ε (Bharathi et al., 2014).

The sign function defined as follows:

$$sign(s) = \left\{ \begin{array}{c} 1, s > 0 \\ 0, s = 0 \\ -1, s < 0 \end{array} \right\} \tag{4.18}$$

Consequently, combining Equations (4.16) and (4.17), the input of the control current i_{qref} can be expressed as follows:

$$-\varepsilon\,\mathrm{sgn}(s) - ks = -\left(\frac{3P}{2J}\lambda_m i_{qref} - \frac{B}{J}\omega_r - \frac{Tl}{J}\right) + c\left(\omega_{ref} - \omega_r\right) \tag{4.19}$$

$$i_{qref} = \frac{2J}{3P\lambda_m}\left(\frac{B}{J}\omega_r + \frac{Tl}{J} + \varepsilon\,\mathrm{sgn}(s) + ks + c\left(\omega_{ref} - \omega_r\right)\right) \tag{4.20}$$

4.3.3 Stability Analysis

In order to check the convergence of the ISMC-ERL, a positive definite Lyapunov function (V) is used to check the control stability. The employed Lyapunov function (V) is given as follows:

$$V = \frac{1}{2}s^2 \tag{4.21}$$

In order to ensure the convergence of (V), it is necessary to verify that the derivative of V is negative definite:

$$\dot{V} = s\dot{s} < 0 \tag{4.22}$$

$$\begin{aligned}
\dot{V} &= s\dot{s} \\
V &= s(\dot{\omega}_{ref} - \dot{\omega}_r + ce) \\
V &= s\left\{\dot{\omega}_{ref} - \frac{1}{J}\left(\frac{3P}{2}\lambda_m i_{qref} - B\omega_r - T_L\right) + ce\right\} \\
V &= s\left\{-\varepsilon sign(s) - ks - \frac{3P\lambda_m k}{2J} sign(s)\right\} \\
V &= -\varepsilon|s| - ks^2 - \frac{3P\lambda_m k}{2J}|s| < 0
\end{aligned} \tag{4.23}$$

The obtained calculation results show that $\dot{V}$ is negative definite and the stability is ensured in the sense of Lyapunov.

The simplified, 1st-order problem of keeping the scalar s at zero can now be achieved by choosing the control law u of Equation (4.9) such that outside of S(t) (Slotine et al., 1991)

$$\frac{1}{2}\frac{d}{dt}s^2 \le -\eta|s| \tag{4.24}$$

S(t) will nonetheless be reached in a finite time smaller than [s(t=0)]/η. Indeed, assume for instance that s(t=0)>0, and let t_{reach} be the time required to hit the surface s=0 (Slotine et al., 1991). Integrating (4.24) between t=0 and t=t_{reach} leads to

$$0 - s\left(t = 0\right) = s(t = t_{reach}) - s(t = 0) \leq -\eta(t_{reach} - 0)$$

Which implies that

$$t_{reach} \leq s(t = 0) / \eta$$

One would obtain a similar result starting with $s(t = 0) < 0$, and thus

$$t_{reach} \leq \left|s(t = 0)\right| / \eta \tag{4.25}$$

After substituting the values and solving for the reaching time or this can be found by MATLAB command.

$$t_{reach} = 0.004\sec$$

4.4 Optimization of Controller Parameters with Genetic Algorithm

In this paper, GA is considered to have an optimal linear and nonlinear gain tuner because it is simple to use and understand, and it has almost identical characteristics to that of PSO. As GA optimization is used in this study to tune the controller parameters, one of the fundamental things to define first is the objective function to be minimized. Before thinking about how to tune a controller, we must first determine what constitutes a good response. In fact, there are a variety of measures that can be used to compare the quality of controlled responses. Those performance measures are expressed in terms of integral squared error (ISE), integral of time squared error (ITSE), integral absolute error (IAE) and integral of time absolute error (ITAE). As we refer from different paper most of performances measure expressed in terms of integral absolute error (IAE) and integral time absolute error (ITAE). Integral time absolute error (ITAE) is mathematically expressed as in equation 4.26.

$$ITEA = \int_{t=0}^{t=tf} t\left|e(t)\right| dt \tag{4.26}$$

ISMC-ERL for speed control and PI for current controller has five tuning parameters such as Kp, Ki, k1, k2 and k3. To tune the parameters of the proposed controller ITAE used as an objective function. The details of GA optimization parameters setting used in simulation for tuning ISMC-ERL speed controller of PMSM drive is shown in Table 4.1.

Table 4.1: Parameter settings of GA optimization for NPID controller

Parameter	Type and value
Population size	30
Maximum generation	50
Number of variables	5
Lower bound	[0 0 0 0 0]
Upper bound	[50 50 100 100 100]

The graphical result of the optimized object function (ITAE) for parameter tuning of ISMC-ERL controller is shown in Figure 4.1. The best value after optimization is 0.150311.

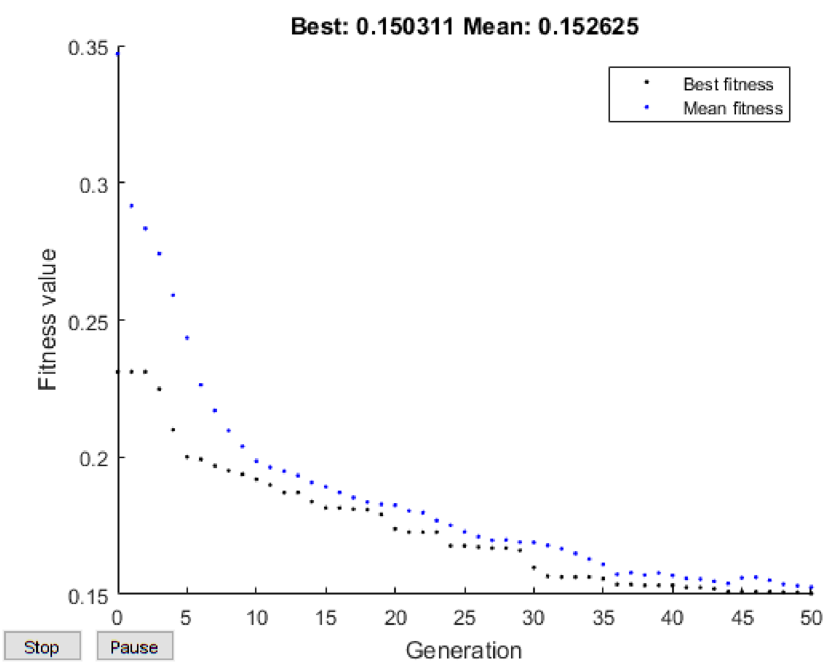

Figure 4.1 Fitness Values vs Generation for Object Function (ITAE)

CHAPTER FIVE

RESULT AND DISCUSSION

5.1 Overview

In this chapter, a thorough Simulink model for a three-wheeled electric Bajaj's Integral Sliding Mode Control with Exponential Reaching aw (ISMC-ERL) is designed using MATLAB/Simulink R2017a. The effectiveness of the controller (ISMC-ERL) is confirmed by means of the model through comparisons with SMC and PID controllers under various conditions. Figure 5.1 depicts the overall Simulink model employed for control system design and performance evaluation.

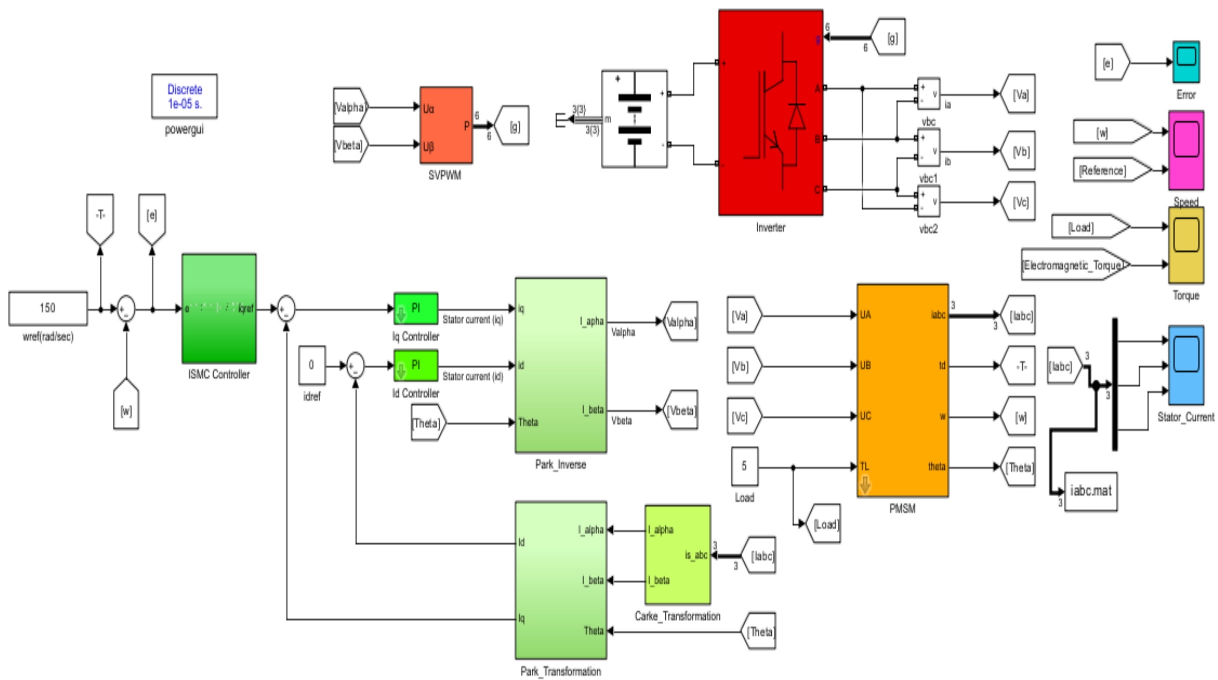

Figure 5.1: Simulink PMSM Drive Model.

5.2 Simulation Results

The suggested ISMC-ERL speed controller for a PMSM drive and a PI current controller for controlling the d and q coordinates currents are presented in this section's simulation results. Analysis is done on the matching three-phase stator current and electromagnetic torque generated. Simulations were performed with various setpoint and load torque settings to assess the effectiveness of the various speed and current controller.

Using 157 rad/s as a reference, Figure 5.2 displays the motor's speed response.

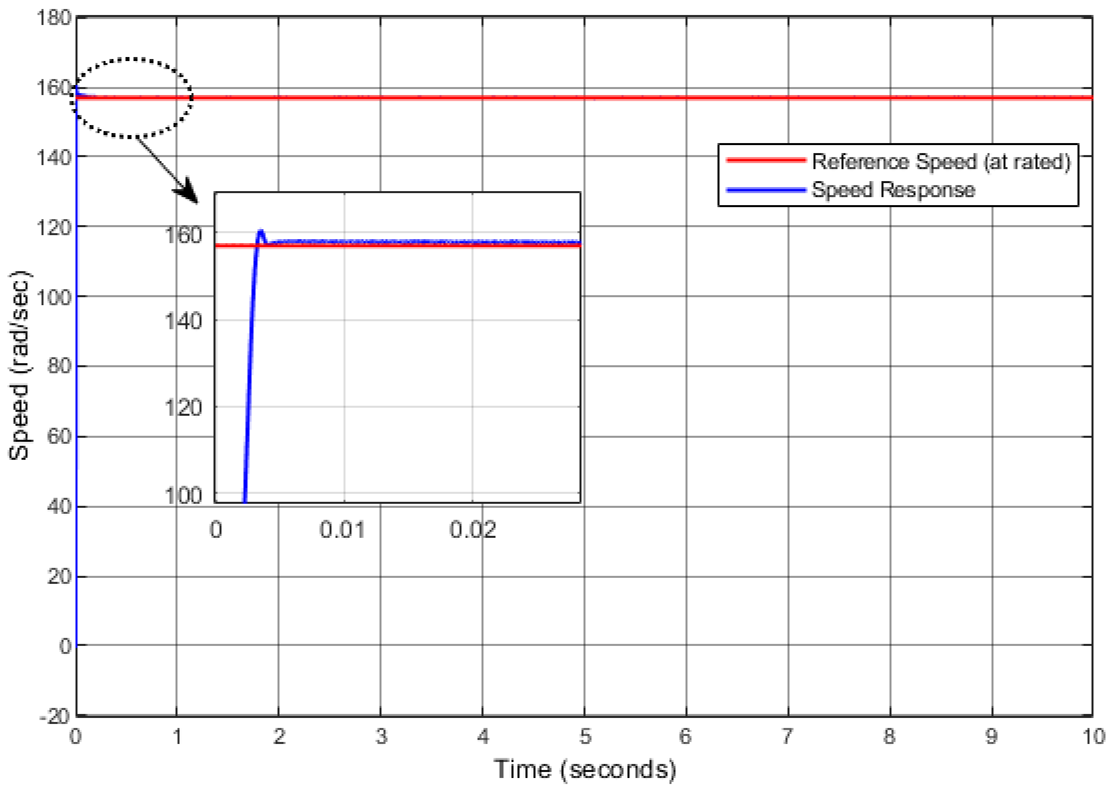

Figure 5.2: PMSM Speed Output at Rated Speed (157 rad/s) Under No-Load Conditions

Figure 5.2 demonstrates that the rotor speed effectively tracks the reference input signal using the proposed ISMC controller. The system achieves with a rising time of 0.0019 seconds, a settling time of 0.0032 sec, and an overshoot of 1.67% at the rated speed of 157 rad/s. These simulation findings validate the ISMC controller's efficacy.

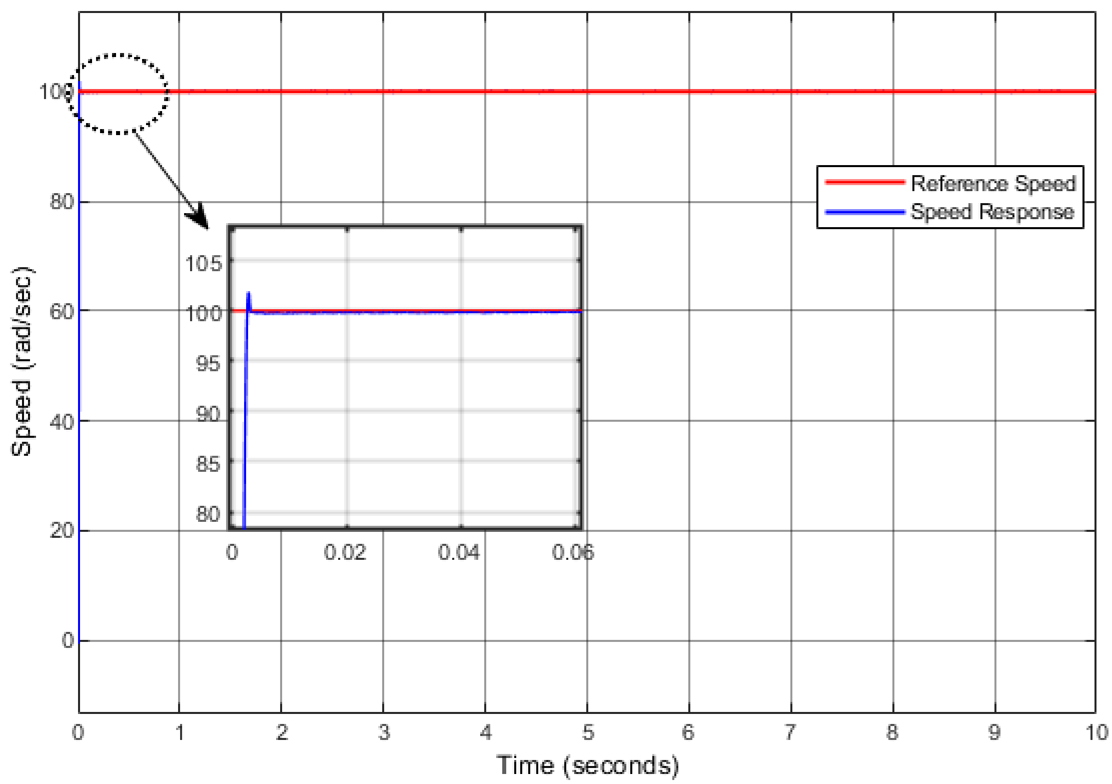

Figure 5.3: PMSM Speed Output at 100 rad/s at T_L=3Nm Conditions

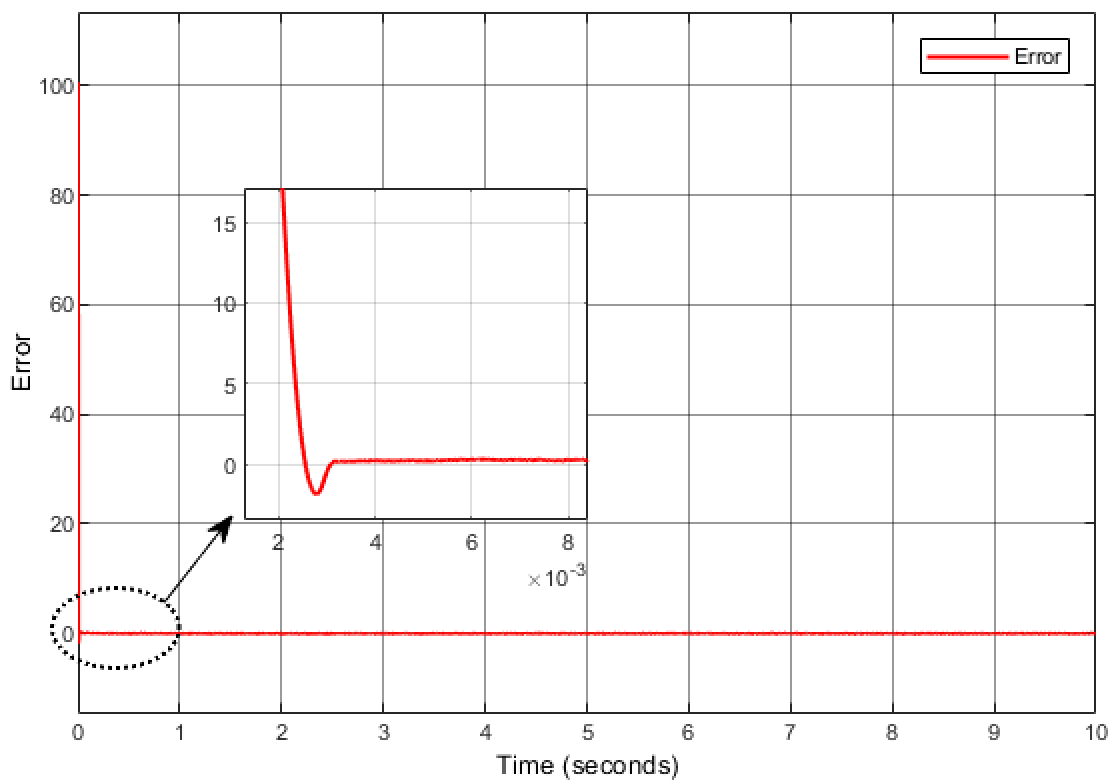

Figure 5.4: The PMSM's speed error at T_L=3Nm Conditions

Figure 5.5 demonstrates the suggested integral sliding mode controller's (ISMC) performance with a variable speed input. An ISMC based on the exponent reaching law (ERL) is employed to regulate the PMSM drive's rotor speed. The results demonstrate accurate tracking of the specified reference input by the motor's rotor speed.

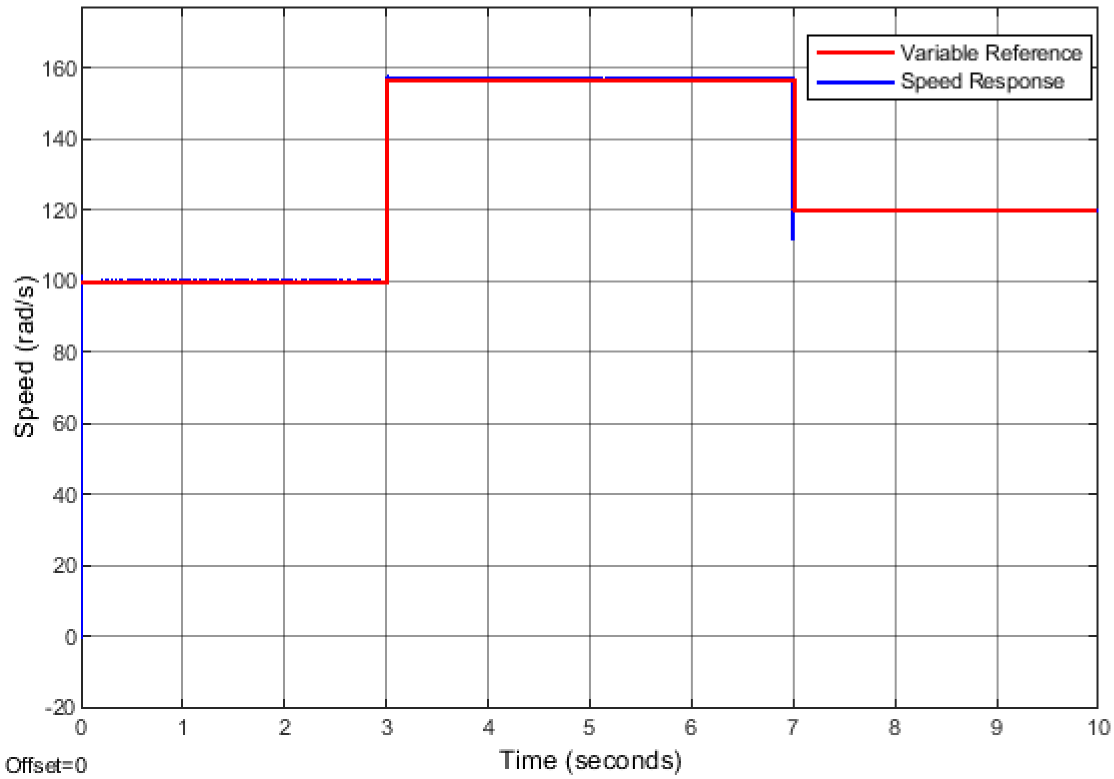

Figure 5.5: PMSM Speed Output at Variable Speed: No-Load Conditions

Figure 5.6 demonstrates the three phase stator currents (i_a, i_b and i_c) drawn by the motor when the motor is operating at a reference speed. Initially, the current exhibits a non-sinusoidal waveform before transitioning to a sinusoidal pattern as the motor reaches steady state under controller command. The strength of the three-phase current is influenced by the external load on the motor.

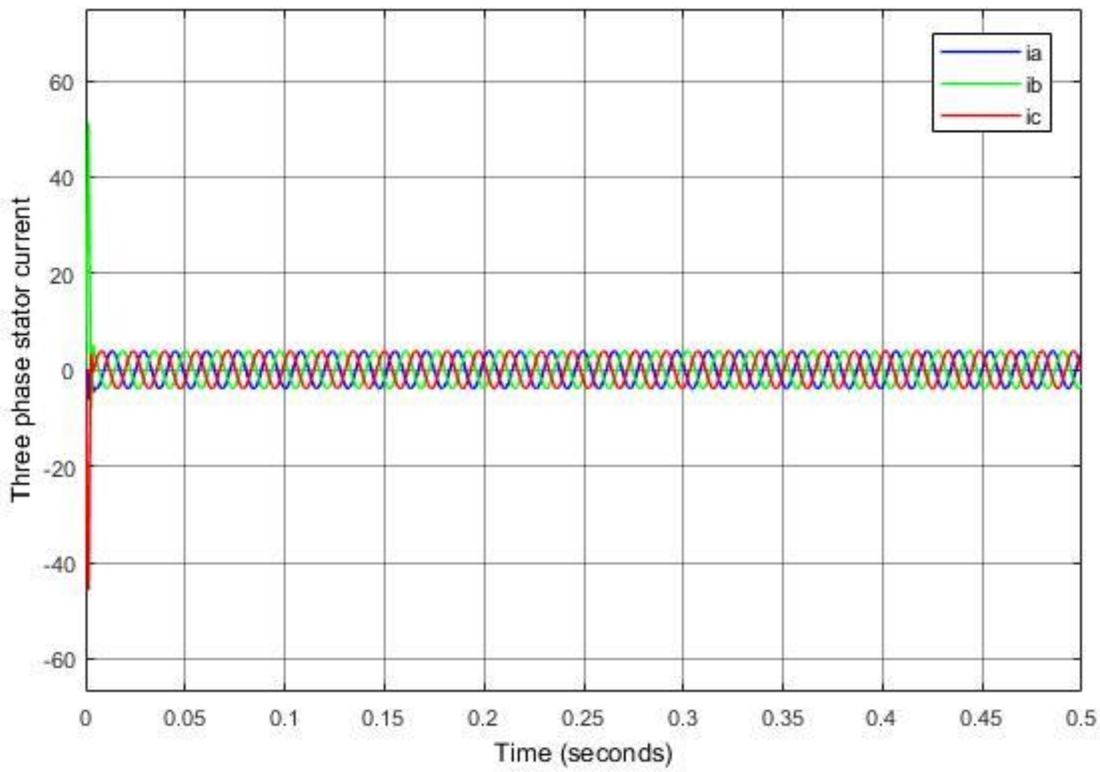

Figure 5.6: i_a, i_b and i_c currents as motor accelerating to rated speed at T_L=5Nm

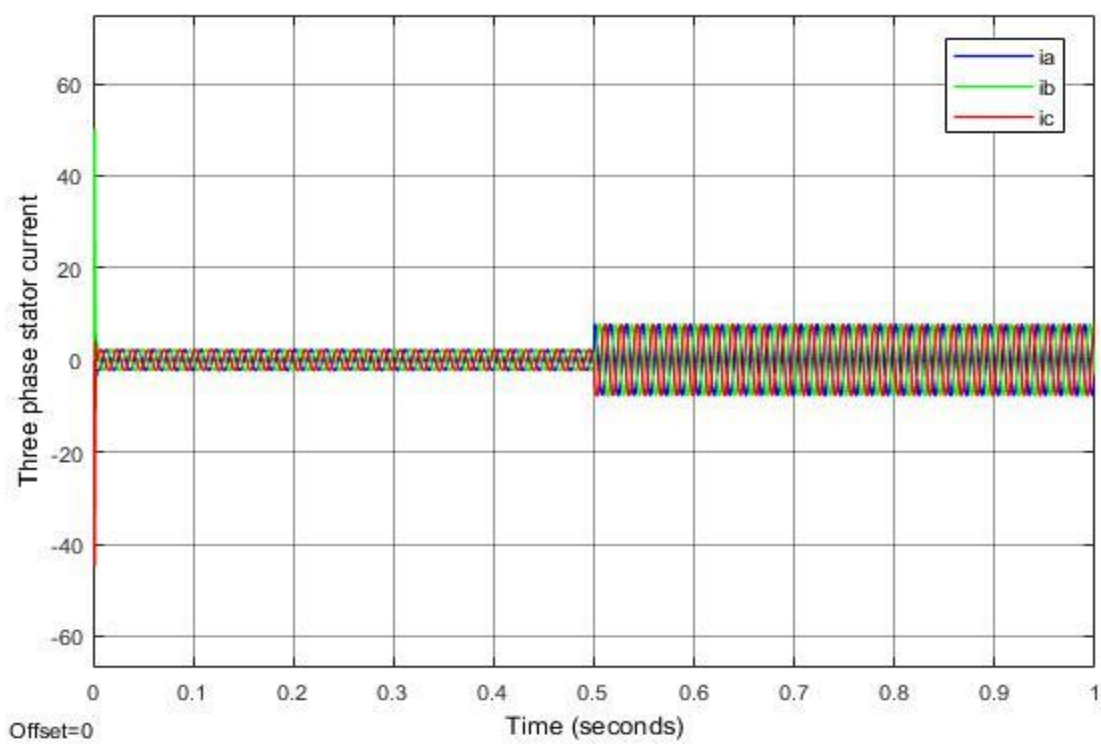

Figure 5.7: Three phase current generate from PMSM with load

The three-phase stator current waveform at t = 0.5 seconds with a 10 Nm load force applied is shown in Figure 5.7. For maximum torque production, as mentioned in Chapter 3, vector control is set to zero, lining up the three-phase stator current with the q- axis stator current((i_q)). As a result of the higher load torque, Figure 5.7 simulation results demonstrate a comparable increase in the three-phase current's magnitude at t = 0.5 seconds.

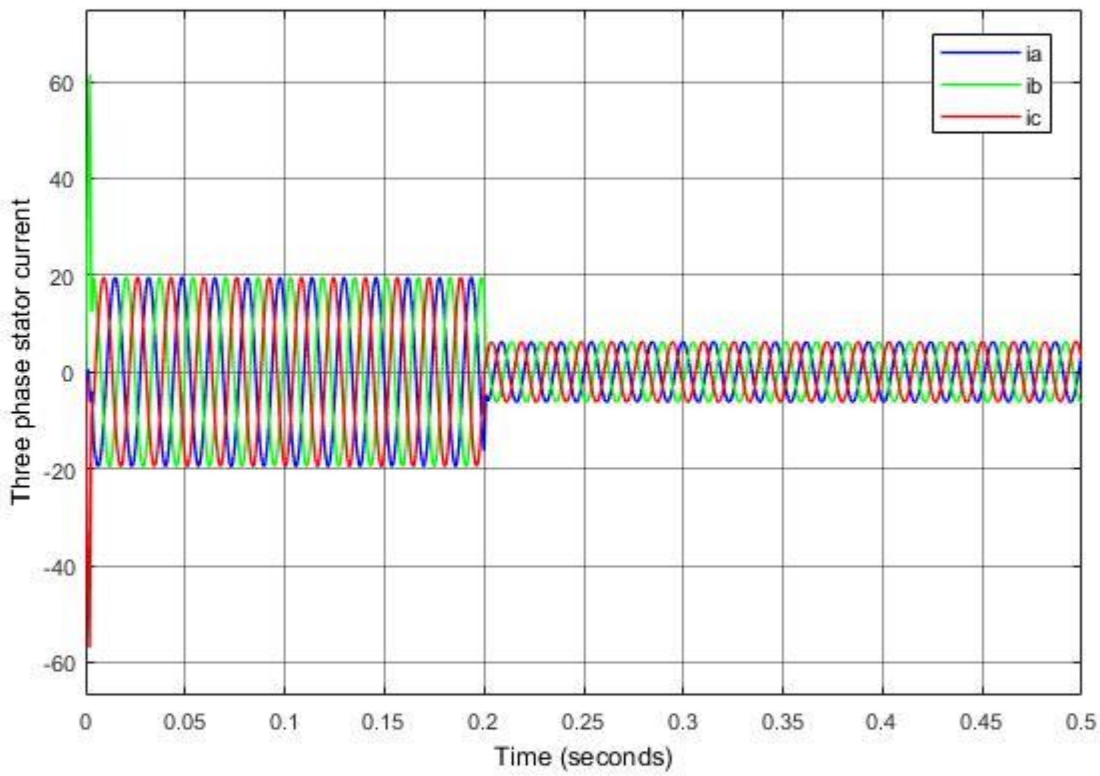

Figure 5.8: Three phase stator current at 20Nm TL and settling time at 0.2

Figure 5.9 demonstrates the electromagnetic torque that has been created. The main cause of the initial torque spike is the rotor's acceleration to a steady speed of 100 rad/s. The steady-state value is not met by this peak torque. In the absence of load torque (T_L=0), the generated torque is solely used to overcome accelerating and frictional forces. However, after approximately 0.005 seconds, the generated torque nearly vanishes as only minimal friction needs to be counteracted.

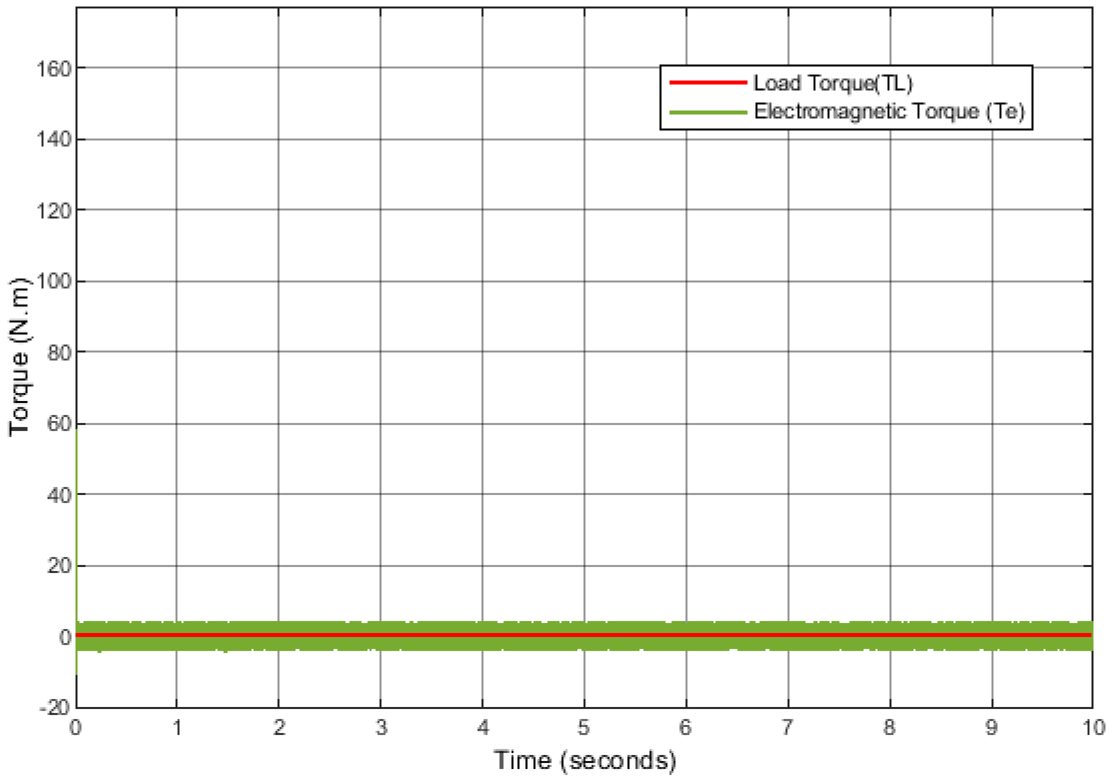

Figure 5.9: Developed electromagnetic torque for input load 0 Nm TL

According to the Figure 5.10, it demonstrates that the torque response under variable torque load. A 10 Nm load is applied to the motor initially, and after 3 seconds, it surges to 20 Nm. After 7 seconds, the 20 Nm load is removed.

In Figure 5.11 shows in testing the robustness of the proposed ISMC-ERL control strategy under parameter variations. The stator resistance, stator inductance and the moment of inertia have been multiplied firstly by two and secondly by three, it can be seen that the motor speed tracks its reference value under the existence of parameter variations with good tracking performances.

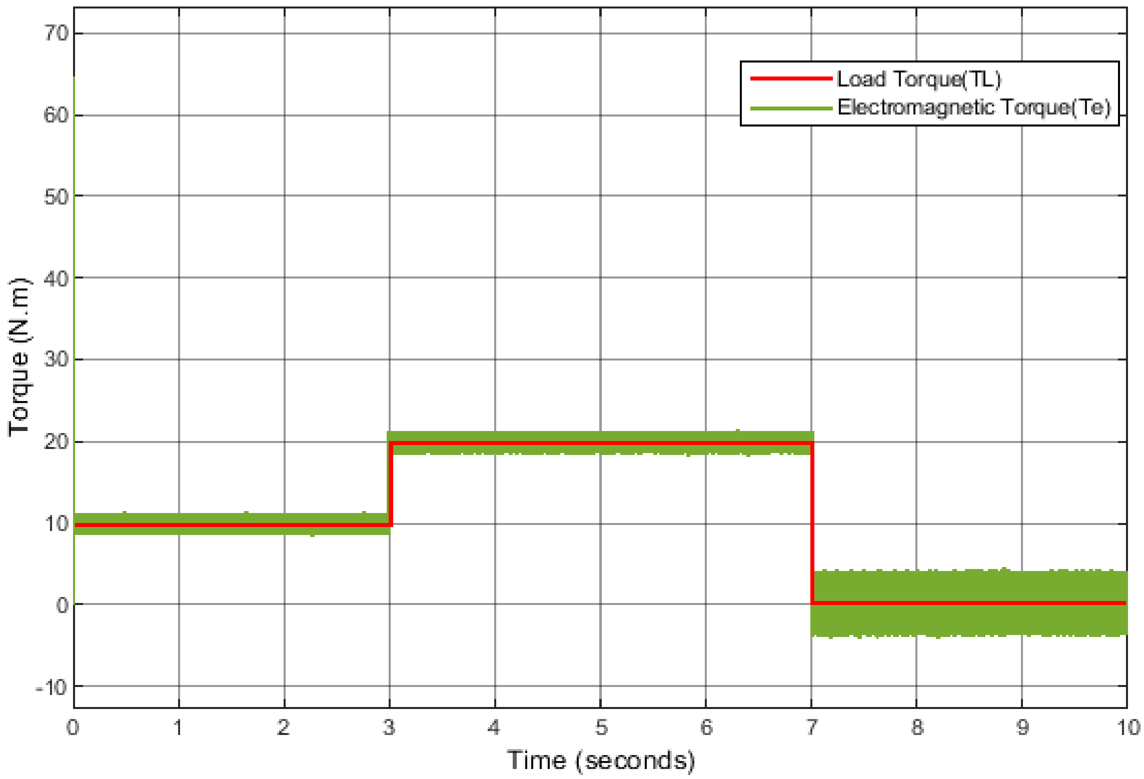

Figure 5.10: Electromagnetic Torque at Variable Load Torque

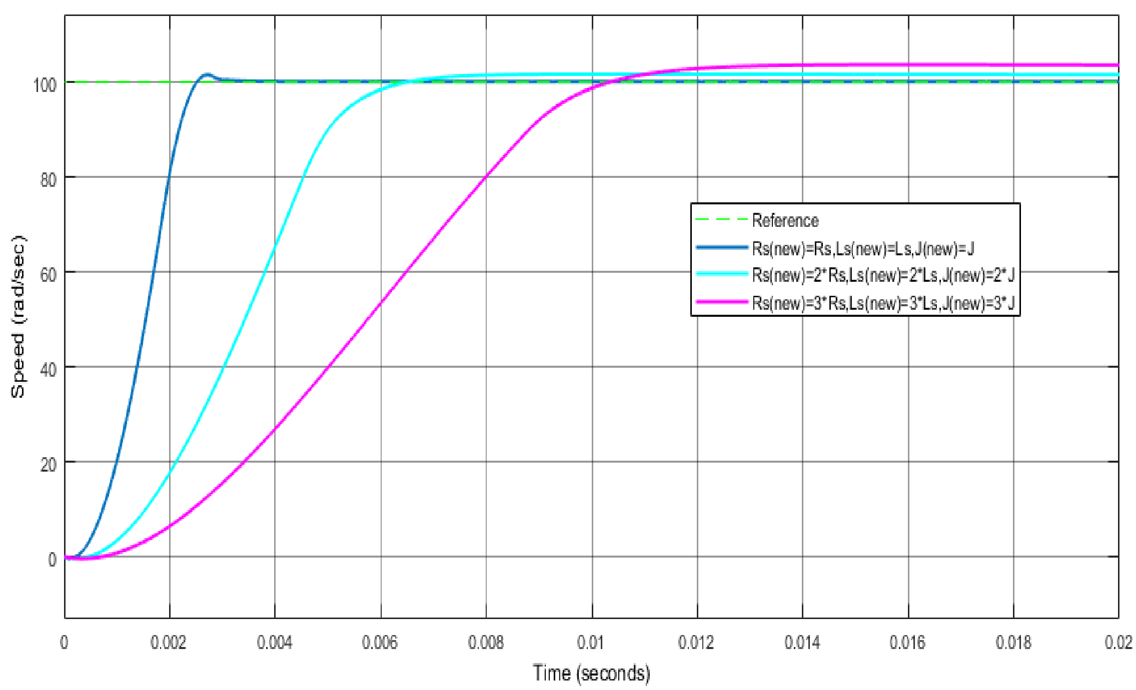

Figure 5.11: Robustness Test and Motor Speed Response Under Parameter Variations

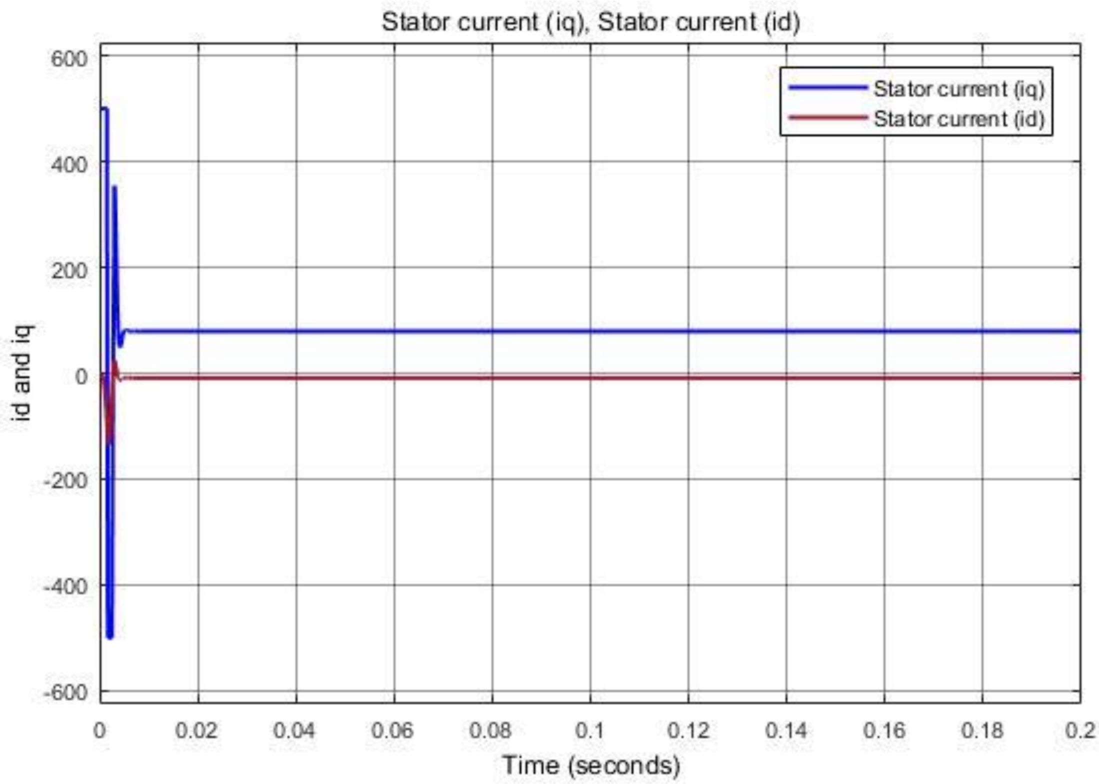

Figure 5.12: Direct and quadrature current result at rated speed

Figure 5.12 displays the simulation findings for i_d and i_q stator currents under a constant 3 Nm load at rated speed. When the q-axis current, which produces torque, has a high beginning value to achieve the desired rotor speed, the PI controller efficiently drives the d-coordinate current to zero. The motor stabilizes the quadrature current once it achieves steady state.

5.3 Controller Performance Comparison at Constant Speed

To evaluate the dynamic performance of different controllers, a comparative analysis was conducted running at 157 rad/s with zero load. Figure 5.13 illustrates the speed responses of the ISMC-ERL, SMC, and PID controllers. To evaluate performance under varying conditions, a variable speed test with load was performed.

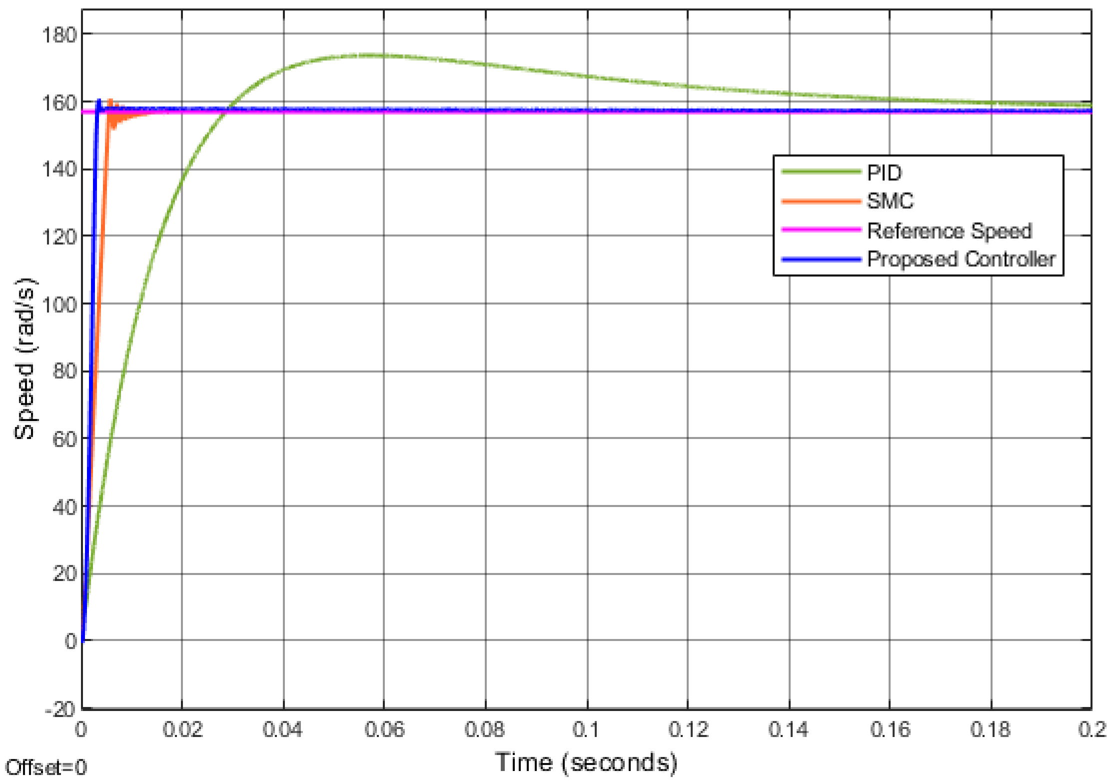

Figure 5.13: PMSM Speed Response: A Comparison of Controllers at 100 rad/s and No Load

Figure 5.14 depicts the speed responses of the controllers under these conditions. The drive system initiated at 100 rad/s and stepped to 157 rad/s at t = 0.4 s then the motor's speed dropped to roughly 120 rad/s at t=0.7 s. The subsequent figures illustrate the machine's speed response for each controller (ISMC-ERL, SMC, and PID) under this variable speed scenario.

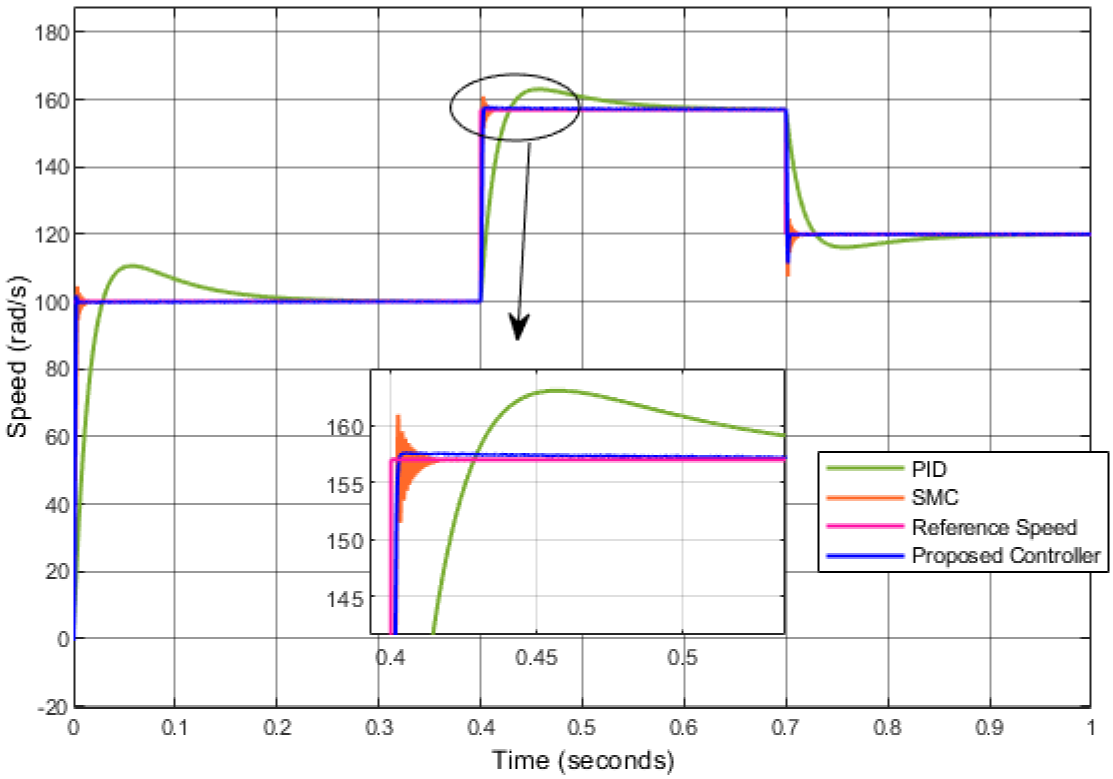

Figure 5.14: Speed response at variable speed and load condition with different controller

The dynamic performance of each controller was evaluated using step response data obtained from the command window. Table 5.1 provides an overview of the generated metrics.

Table 5.1. Comparing Controller Performance at a Speed of 157 rad/s

Types of Controllers	System Performance			
	Rise time (sec)	Settling time (sec)	Overshoot (%)	Torque Ripple
ISMC-ERL	0.0019	0.0032	1.67	14.34
PID	0.0207	0.1434	9.35	19.62
SMC	0.0041	0.0078	2.37	17.15

CHAPTER SIX

CONCLUSION AND RECOMMENDATION

6.1 Conclusion

This research investigated the speed control of a PMSM for electric vehicles (EVs) using an ISMC-ERL controller in the speed loop and two PI controllers in the current loop. ISMC-ERL is a cutting-edge control technique that outperforms traditional methods in terms of precision and robustness. It effectively addresses challenges like overshoot, undershoot, parameter variations, and external disturbances, ensuring reliable and efficient operation for electric vehicles. Results indicate that the proposed controller effectively regulates PMSM speed, demonstrating superior robustness to external disturbances compared to traditional control methods. The proposed controller significantly enhances speed regulation, dynamic response, accuracy, and stability.

A detailed MATLAB/Simulink model was developed to simulate the EV system, encompassing the ISMC-ERL controller, coordinate transformations, SVPWM, inverter, and PMSM. The simulation results confirmed the system's quick response and reliable performance.

6.2 Recommendation

While this thesis explores several key concepts and analyses, certain avenues of research were not pursued due to time constraints. These several avenues for future research and practical applications are identified:

- Enhancing SMC performance through advanced tuning techniques and exploring hybrid control strategies with MPC or fuzzy logic are recommended.
- Practical implementation necessitates hardware optimization, efficient real-time algorithms, and rigorous experimental validation.
- Integrating IoT and AI technologies offers potential for advanced control, monitoring, and predictive maintenance.

Addressing these areas will play a role in designing more efficient, reliable, and adaptable PMSM speed control systems.

REFERENCES

Abu-Rub, H., Iqbal, A., & Guzinski, J. (2021). *High Performance Control AC Drives with MATLAB®/Simulink*. https://doi.org/10.1002/9781119591313

Bello, A., Kilishi, I., Bari, M., & Usman, A. (2020). Comparative Review On PMSM And BLDCM Based On Direct Torque Control Method. *Journal of Manufacturing Technology Research*.

Bennett, S. (1994). Development of the PID Controller. *Control Systems, IEEE*. https://doi.org/10.1109/37.248006

Benzaouia, S., M'Sirdi, N., Rabhi, A., & Naamane, A. (2022). Integral Sliding Mode Control with Exponential Reaching law for PMSM in Electric Vehicles. *IFAC-PapersOnLine*, *55*(12), 222–227. https://doi.org/https://doi.org/10.1016/j.ifacol.2022.07.315

Bharathi, N., Kavitha, Dr. A., & Barathy, B. (2014). *SLIDING MODE CONTROL FOR SPEED CONTROL OF BRUSHLESS DC MOTOR*. https://api.semanticscholar.org/CorpusID:212506802

Bhatt, P. M., Mehar, H., & Sahajwani, M. (2019). Electrical Motors for Electric Vehicle – A Comparative Study. *SSRN Electronic Journal*. https://api.semanticscholar.org/CorpusID:216639217

Blaha, P., & Václavek, P. (2012). Robust control of permanent magnet synchronous motor. *2012 12th International Conference on Control, Automation and Systems*, 1317–1322. https://api.semanticscholar.org/CorpusID:7360982

Boby, K., & Kottalil, A. M. (2013). *Simulation of PMSM Vector Control System with Fuzzy Self-Adjusting PID Controller Using MATLAB*. https://api.semanticscholar.org/CorpusID:16942110

Cao, R., Mi, C., & Cheng, M. (2012). Quantitative Comparison of Flux-Switching Permanent-Magnet Motors With Interior Permanent Magnet Motor for EV, HEV, and PHEV Applications. *Magnetics, IEEE Transactions On*, *48*, 2374–2384. https://doi.org/10.1109/TMAG.2012.2190614

Castanos, F., & Fridman, L. (2006). Analysis and design of integral sliding manifolds for systems with unmatched perturbations. *IEEE Transactions on Automatic Control*, *51*(5), 853–858. https://doi.org/10.1109/TAC.2006.875008

Chauhan, S. (2015). Motor Torque Calculations For Electric Vehicle. *International Journal of Scientific & Technology Research*, *4*, 126–127. https://api.semanticscholar.org/CorpusID:106418790

Colak, I., Kabalcı, E., & Bayindir, R. (2011). Review of multilevel voltage source inverter topologies and control schemes. *Energy Conversion and Management*, *52*, 1114–1128. https://doi.org/10.1016/j.enconman.2010.09.006

Deo, H. V, & Shekokar, R. U. (2015). *Simulation of PMSM Speed Control System with Vector Control Method based on Matlab*. www.allsubjectjournal.com

Ding, Z., Wei, G., & Ding, X. (2014). Speed identification and control for permanent magnet synchronous motor via sliding mode approach. *Systems Science & Control Engineering: An Open Access Journal*, *2*, 161–167. https://doi.org/10.1080/21642583.2014.886974

Efe, M. Ö. (2011). Fractional Order Systems in Industrial Automation—A Survey. *IEEE Transactions on Industrial Informatics*, *7*(4), 582–591. https://doi.org/10.1109/TII.2011.2166775

Eker, İ. (2010). Second-order sliding mode control with experimental application. *ISA Transactions*, *49*(3), 394–405. https://doi.org/https://doi.org/10.1016/j.isatra.2010.03.010

Hamayun, M. T., Edwards, C., & Alwi, H. (2016). Integral sliding mode control. In *Studies in Systems, Decision and Control*. Springer International Publishing. https://doi.org/10.1007/978-3-319-32238-4_2

Hashemnia, M. N., & Asaei, B. (2008). *Comparative study of using different electric motors in the electric vehicles*. https://doi.org/10.1109/ICELMACH.2008.4800157

Huang, J., Cui, L., Shi, X., Li, H., & Xiang, Z. (2014). Composite integral sliding mode control for PMSM. *Proceedings of the 33rd Chinese Control Conference*, 8086–8090.

Jiacai, H., Hongsheng, L., Fulin, T., & Di, L. (2012). Fractional order sliding mode controller for the speed control of a permanent magnet synchronous motor. In *Proceedings of the 2012 24th*

Chinese Control and Decision Conference, CCDC 2012. https://doi.org/10.1109/CCDC.2012.6244192

Kapil Parkh. (2014). Field Oriented Control of PMSM Using Improved Space Vector Modulation Technique. *International Journal of Digital Application & Contemporary Research (IJDACR)*, *2*(8).

Kumar, K., Angel, P., John, J., & Kumar. (2010). Simulation and comparison of SPWM and SVPWM control for three phase inverter. *ARPN Journal of Engineering and Applied Sciences*.

Lee, S.-T. (2009). *Development and Analysis of Interior Permanent Magnet Synchronous Motor with Field Excitation Structure*. https://api.semanticscholar.org/CorpusID:11719652

LEVANT, A. (1993). Sliding order and sliding accuracy in sliding mode control. *International Journal of Control*, *58*(6), 1247–1263. https://doi.org/10.1080/00207179308923053

Li, J., Ren, H., Wang, S., & Fang, Y. (2020). *Integral Sliding Mode Control for PMSM with Uncertainties and Disturbances via Nonlinear Disturbance Observer*.

Liang, W., Wang, J., Luk, P., Fang, W., & Fei, W. (2014). Analytical Modeling of Current Harmonic Components in PMSM Drive With Voltage-Source Inverter by SVPWM Technique. *Energy Conversion, IEEE Transactions On*. https://doi.org/10.1109/TEC.2014.2317072

Liu, T., Chen, G., & Li, S. (2015). Application of Vector Control Technology for PMSM Used in Electric Vehicles. *The Open Automation and Control Systems Journal*, *6*, 1334–1341. https://doi.org/10.2174/1874444301406011334

Liuping, W., Shan, C., Dae, Y., Lu, G., & Ki, N. (2015). *PID AND PREDICTIVE CONTROL OF ELECTRICAL DRIVES AND POWER CONVERTERS USING MATLAB ® /SIMULINK ®*.

Maji, P., KPanda, P., & KSaha, P. (2015). Field Oriented Control of Permanent Magnet Synchronous Motor Using PID Controller. *International Journal of Advanced Research in Electrical, Electronics and Instrumentation Engineering*, *04*, 632–639. https://doi.org/10.15662/ijareeie.2015.0402019

Mehrdad, E., Yimin, G., & Ali, E. (2005). *Modern electric, hybrid electric and fuel cell vehicles* (1st ed.). Fundamentals, Theory, and Design. Boca Raton, FL: CRC, 2005.

Mohd Zaihidee, F., Mekhilef, S., & Mubin, M. (2019). Application of Fractional Order Sliding Mode Control for Speed Control of Permanent Magnet Synchronous Motor. *IEEE Access*. https://doi.org/10.1109/ACCESS.2019.2931324

Mujumdar, A., Tamhane, B., & Kurode, S. (2015). Observer-Based Sliding Mode Control for a Class of Noncommensurate Fractional-Order Systems. *IEEE/ASME Transactions on Mechatronics*, *20*(5), 2504–2512. https://doi.org/10.1109/TMECH.2014.2386914

Nam, K. (2018). *AC Motor Control and Electrical Vehicle Applications*. https://doi.org/10.1201/9781315200149

Nanda, G., & Kar, N. (2006). A Survey and Comparison of Characteristics of Motor Drives Used in Electric Vehicles. In *Canadian Conference on Electrical and Computer Engineering*. https://doi.org/10.1109/CCECE.2006.277736

Parmar, Y., Patel, P., Pancholi, N., Thakor, C., & Mali, U. (2016). Scalar control of Permanent Magnet Synchronous motor. *International Research Journal of Engineering and Technology*. www.irjet.net

Pathak, D., Sagar, G., & Gaur, P. (2020). An Application of Intelligent Non-linear Discrete-PID Controller for MPPT of PV System. *Procedia Computer Science*, *167*, 1574–1583. https://doi.org/10.1016/j.procs.2020.03.368

R., S., & Rajagopal, K. (2016). *An Insight into Motor and Battery Selections for Three-Wheeler Electric Vehicle*. https://doi.org/10.1109/ICPEICES.2016.7853494

Ramu Krishnan. (2017). *Permanent Magnet Synchronous and Brushless DC Motor Drives* (1st ed.). CRC Press.

Ren, W., Wu, Y., & Du, R. (2020). *A Vector Control System of PMSM with the Assistance of Fuzzy PID Controller*. https://doi.org/10.23919/CCC50068.2020.9189325

Rodriguez, J., Pontt, J., Silva, C., Correa, P., Lezana Illesca, P., Cortes, P., & Ammann, U. (2007). Predictive Current Control of a Voltage Source Inverter. *Industrial Electronics, IEEE Transactions On*, *54*, 495–503. https://doi.org/10.1109/TIE.2006.888802

Sharifian, M. B. B., Herizchi, T., & Firouzjah, K. (2009). Field oriented control of permanent magnet synchronous motor using predictive space vector modulation. In *2009 IEEE Symposium on Industrial Electronics and Applications, ISIEA 2009 - Proceedings*. https://doi.org/10.1109/ISIEA.2009.5356385

Slotine, Jean-Jacques E., & Weiping Li. (1991). Applied nonlinear control. Vol. 199. No.1., Englewood Cliffs, NJ: Prentice-Hall, 281-282.

Suman, K., & Mathew, A. (2018). *Speed Control of Permanent Magnet Synchronous Motor Drive System Using PI, PID, SMC and SMC plus PID Controller*. https://doi.org/10.1109/ICACCI.2018.8554788

Utkin, V., & Shi, J. (1996). Integral sliding mode in systems operating under uncertainty conditions. *Proceedings of 35th IEEE Conference on Decision and Control*, *4*, 4591–4596.

Vidhya, D., & Mahadevan, B. (2019). Modelling, design and control of a light electric vehicle with hybrid energy storage system for Indian driving cycle. *Measurement and Control - London- Institute of Measurement and Control-*. https://doi.org/10.1177/0020294019858212

Wang, L., Yu, B., Du, H. B., Wu, D., Zhu, W., & Ding, S. (2020). Speed Regulation for PMSM Based on Fixed-time Sliding Mode Control. *IECON Proceedings (Industrial Electronics Conference)*, *2020-October*, 5105–5109. https://doi.org/10.1109/IECON43393.2020.9254968

Wu, H., Su, W., & Liu, Z. (2014). PID controllers: Design and tuning methods. In *Proceedings of the 2014 9th IEEE Conference on Industrial Electronics and Applications, ICIEA 2014*. https://doi.org/10.1109/ICIEA.2014.6931273

Xia, C., Wang, X., Li, S., & Chen, X. (2011). Improved integral sliding mode control methods for speed control of PMSM system. *International Journal of Innovative Computing, Information and Control*, *7*.

Yong, L. (2017). *Vector Control of Permanent Magnet Synchronous Motor for Fan of New Energy Vehicle*. https://api.semanticscholar.org/CorpusID:56219825

Young, K. D., Utkin, V. I., & Ozguner, U. (1999). A control engineer's guide to sliding mode control. *IEEE Transactions on Control Systems Technology*, *7*(3), 328–342. https://doi.org/10.1109/87.761053

Zaihidee, F. M., Mekhilef, S., & Mubin, M. (2019). Robust speed control of pmsm using sliding mode control (smc)-a review. In *Energies* (Vol. 12, Issue 9). MDPI AG. https://doi.org/10.3390/en12091669

Zambada, J., & Deb, D. (2010). *Sensorless Field Oriented Control of a PMSM*. www.microchip.com

Zeraoulia, M., Benbouzid, M., & Diallo, D. (2006). Electric Motor Drive Selection Issues for HEV Propulsion Systems: A Comparative Study. *Vehicular Technology, IEEE Transactions On*, *55*, 1756–1764. https://doi.org/10.1109/TVT.2006.878719

Zhang, X., Sun, L., Zhao, K., & Sun, L. (2013). Nonlinear Speed Control for PMSM System Using Sliding-Mode Control and Disturbance Compensation Techniques. *IEEE Transactions on Power Electronics*, *28*(3), 1358–1365. https://doi.org/10.1109/TPEL.2012.2206610

Appendix

A. Comparing Controller Performance

<table>
<tr><td colspan="2">RiseTime: 0.0019
TransientTime: 0.0032
SettlingTime: 0.0032
SettlingMin: 142.2499
SettlingMax: 160.5681
Overshoot: 1.6709
Undershoot: 0.3735
Peak: 160.5681
PeakTime: 0.0035

ans =

'Speed Performance of ISMC-ERL'</td></tr>
<tr><td>RiseTime: 0.0207
TransientTime: 0.1434
SettlingTime: 0.1434
SettlingMin: 142.9716
SettlingMax: 173.6892
Overshoot: 9.3543
Undershoot: 0
Peak: 173.6892
PeakTime: 0.0572

ans =

'Speed Performance of PID'</td><td>RiseTime: 0.0041
TransientTime: 0.0078
SettlingTime: 0.0078
SettlingMin: 141.5153
SettlingMax: 160.7300
Overshoot: 2.3764
Undershoot: 0.1626
Peak: 160.7300
PeakTime: 0.0058

ans =

'Speed Performance of SMC'</td></tr>
</table>

Table A.1: Comparing Controller Performance at Speed 157 rad/s

B. α-β to A-B-C Simulink Model

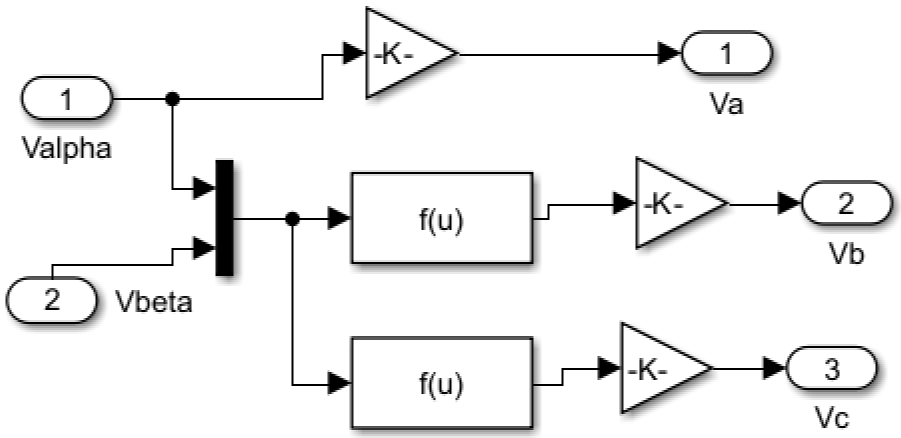

Figure B.1: α-β to A-B-C Simulink Model

C. D-Q to α-β Simulink Model

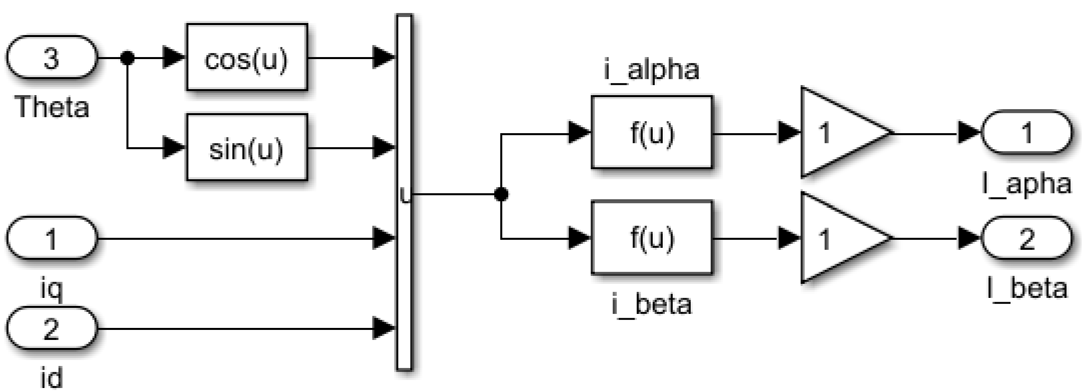

Figure C.2: D-Q to α-β Simulink Model

D. Simulink model for PMSM

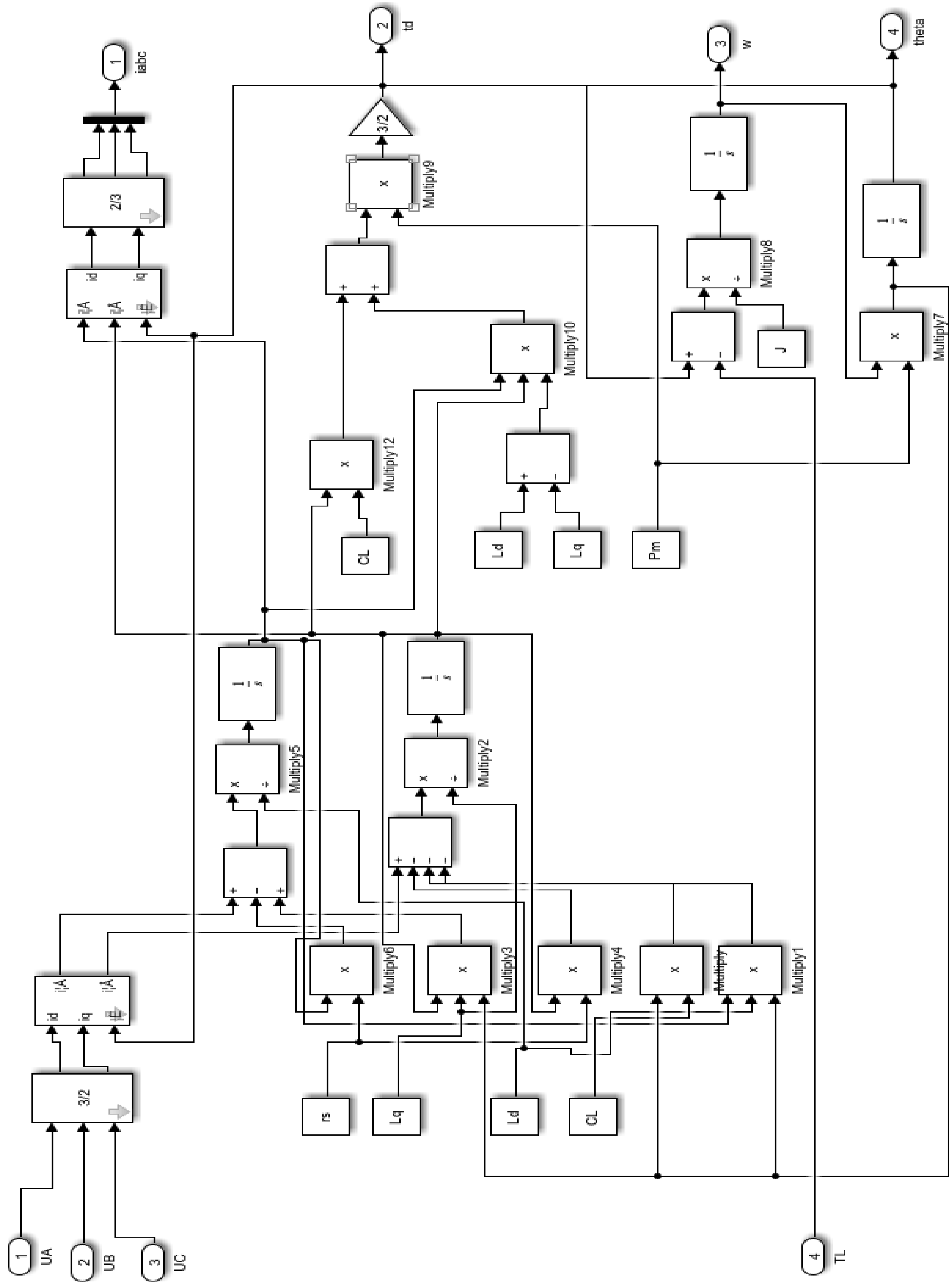

Figure D.3: Simulink model for PMSM

Sign.Plus by Alohi

Document ID: 66e98be60926ac0f7f9d5be5
Document Name: Hamza Abdo Thesis(17.9.2024)
Document Pages: 85

Document Status: Completed
Document Completion Date: September 17, 2024, 14:04 UTC

Signer: almaz (almaztekle24@gmail.com)

Signer	Signature	Timestamps
almaz almaztekle24@gmail.com Using IP: 196.190.62.233 IP Location: Ethiopia, Addis Ababa Authentication method: Email		Viewed: September 17, 2024, 14:04 UTC Signed: September 17, 2024, 14:04 UTC